

**Proceedings of conference on Advancement in Computation,
Communication and Electronics Paradigm (ACCEP-2019)**

18th January, 2019

Organised by

Department of Computer Science & Electronics

Ramakrishna Mission Vidyamandira, Belur Math, Howrah

Published by:

Swami Shastrajnananda
Principal
Ramakrishna Mission Vidyamandira
Belur Math, Howrah, 711202
Phone: (033) 2654-9181
Email: vidyamandira@gmail.com

18 January 2019

Editors :

Mr. Sarbajit Manna
Mr. Avishek Barman
Dr. Ranjit Das
Dr. Atanu Mondal
Dr. Arindam Sarkar

ISBN : 978-81-940096-0-3

Printed at:

Bengal Printing Works
51, R. N. Bhattacharjee Street
Belur Math, Howrah, 711202
Phone: 9831616768

Contents

Preface

Publisher's Note

Abstract of Invited Paper

- Role of Computing in Greener World: From Desktop to Cloud Based Solutions 1
Dr. Sunirmal Khatua

Technical Papers

- A Survey on Image Segmentation Techniques 2
Rozina Khatoon and Dr. Abhishek Das
- Noisy Gene Expression and Its Benefit 10
Dr. Rajesh Karmakar
- Face Detection and Eye Extraction using Canny Edge Detection and Hough Transform 14
Dildar Ali and Dr. Abhishek Das
- Study on Supercontinuum in Dispersion Engineered Silicon Nanowire 19
Ranjit Das
- Energy Harvesting Mechanism for Network/Device 23
Dujendu Kumar Chowdhury, Bishal Kumar Saha, Indranil Saha, Manish Agarwal, and Swarup Kumar Mitra
- Impact of Data Normalization on Deep Neural Network for Time Series Forecasting 27
Samit Bhanja and Dr. Abhishek Das
- Reversibility of α – Asynchronous Cellular Automata: A Simulation-Based Study 32
Anupam Pattanayak and Subhasish Dhal
- Detection of Fabrication, Replay and Suppression Attack in VANET- A Database Approach 38
Atanu Mondal and Mayurakshi Jana

Preface

The real-life problems faced by humanity can be catered by the technological advancements in computation, communication and electronics engineering based solutions. The main aim of computational and instrumentation methodologies are to provide resilient solutions for these problems. The applications comprise of the different technologies in the fields of computer networking and data communication, cyber security, signal processing, computer vision and image processing, computational perception and cognition, human–computer interaction, adaptive computation and machine learning, analog electronics, digital electronics, consumer electronics, embedded systems, power electronics and many more.

This volume of ACCEP consists of accepted papers presented at ACCEP-2019, the first conference on Advancement in Computation, Communication and Electronics Paradigm 2019. It is aimed to introduce as much as possible the latest trends in advanced computing, communication and electronics based technologies. The aforementioned conference is the first of its kind which will be hosted by the Department of Computer Science and Electronics, Ramakrishna Mission Vidyamandira, Belur Math, Howrah.

We are grateful to Dr. Sunirmal Khatua, Visvesvaraya Young Faculty Fellow, Ministry of Electronics and IT, Govt. of India and Assistant Professor, University of Calcutta, for giving his consent to deliver the keynote address on “Role of Computing in Greener World: From Desktop to Cloud Based Solutions” and grace the occasion.

We would like to express our heartiest thanks to the reviewers of ACCEP 2019, as review process requires a lot of effort. Also, we would like to extend our thanks to all the authors for their superlative contributions. Finally, we would like to express our sincere gratitude and appreciation to the college administration and office staffs of Ramakrishna Mission Vidyamandira, Belur Math, Howrah for their never-ending support in organizing the conference and for making this event a grand success.

**Belur Math, Howrah
18 January 2019**

**Mr. Sarbajit Manna
Mr. Avishek Barman
Dr. Ranjit Das
Dr. Atanu Mondal
Dr. Arindam Sarkar**

Publisher's Note

Computational knowledge is not only a needed constituent in today's learning purview, rather it is playing a crucially significant role in restructuring the model of life style, cultural discourses and expanding the diverse possibilities of human civilization. While the scientist, engineers and technicians are fascinated in finding out innovative paradigms in ethnography of electronically harnessed communication, the common man is marvelled every day with the massive novelty and uniqueness of these outfits in their work-a-day life.

It gives me immense pleasure to note that the Conference Proceedings on Advancement in Computation, Communication and Electronics Paradigm (ACCEP-2019) organized by Department of Computer Science and Electronics of Ramakrishna Mission Vidyamandira is such a challenge to dig out the fresh pitches in this sophisticatedly designed recent age knowledge.

Such a publication will create an opportunity of collaborating dialogues amongst the scholars and will thus consequential in further exploration which is the life signal of any progressive society.

**Belur Math, Howrah
18 January 2019**

Swami Shastrajnananda

Role of Computing in Greener World: From Desktop to Cloud Based Solutions

Dr. Sunirmal Khatua

Visvesvaraya Young Faculty Fellow, Ministry of Electronics and IT, Govt. of India

Assistant Professor, University of Calcutta

Email : enggnimu.ju@yahoo.com

Abstract—Cloud computing has changed the way we compute today. It enables us to access enormous amount heterogeneous resources across the globe in a convenient, on-demand and pervasive way. However, the large-scale virtualized data centers deployed by the Cloud Service Providers (CSPs) like Amazon, Google, IBM consume huge amount of electrical energy. According to latest studies in 2016, data centers were responsible for consumption of about 3% of the global electricity supply and accounted for about 2% of the total greenhouse gas emissions. Analysts predict that by 2025, data centers will consume (1/5)th of the world's total power! This trend gradually increases with the adoption of Internet of Things (IoT), Fog computing and Microservices. Therefore, being computer professional, we have the responsibility to take corrective measures to make our world greener. We need to design Green Cloud computing solutions that not only minimize operational costs but also reduce the environmental impact. The components which consume major energy include Display (33%), CPU (10%), Power Supply (10%) and Memory (9%). In this lecture, I will discuss various approaches to reduce data center energy consumption considering those major components. It will cover various open research challenges, and resource provisioning and allocation algorithms for energy-efficient management of Cloud computing environments.

A Survey on Image Segmentation Techniques

Rozina Khatoon and Abhishek Das, *Member, IEEE*

Abstract—Image segmentation is a process or a technique via which given digital image is segmented into multiple segments in order to multiple analyze each and every of its components present in itself of the image. Image compression or object recognition is the main application of image segmentation because for these types of applications, it is unable to process the whole image. Segmentation mainly used to discover boundaries or edges, object and other related data in the digital image. There are so many various methods are available to perform segmentation like threshold, clustering, edge based method, watershed method etc. based on certain image features like pixel intensity value, color, texture etc. Image segmentation is most popular technique in the area of image processing. The main task of the researchers is to improved a method for efficient in this field and better segmentation. In Image segmentation there are several factors that pretend the process such as the intensity of image to be color segmented, type and noise present in the image. For effective image segmentation, the algorithm development is still a big research that will appear in the area of image processing. Researchers still have to more effort a long term to develop workable algorithm for image segmentation. Here many different image segmentation techniques are reviewed, discussed and comparison based on their advantage and disadvantages.

Index Terms—Image Segmentation, Threshold, Histogram, Watershed

1 INTRODUCTION

IMAGE segmentation is a most important and challenging process of image processing. Image segmentation is technique to partitioning a image on several meaningful parts with similar properties and features based on texture, color, pixel intensity value to represent an digital image into more significant and easy to analyze the image. Image segmentation is the main step of image analysis. Image segmentation is important in many sign processing technique and its applications. The most important methods of image segmentation that can be still used by the researchers that are threshold, side Detection, Histogram, region based methods and Watershed.

Image segmentation is the technique that is widely used in many different fields. The application of image segmentation are: Medical imaging, content based image retrieval, automatic traffic control system, recognition task etc.

- Rozina Khatoon is a M.Tech Student with the Dept. of Computer Science and Engineering, Aliah University, Kolkata, India. Email: rozinakhatoon92@gmail.com
- Dr. Abhishek Das is Associate Professor and Head with the Dept. of Computer Science and Engineering, Aliah University, Kolkata, India. Email: adas@aliah.ac.in

Image segmentation is classified into two simple types: Local segmentation and Global segmentation. The image segmentation algorithms are categorized based on two basic properties of color, gray values or texture those are discontinuity and similarity.

Discontinuity detection based approach:

In discontinuity approach, subdivision or partitioning of a digital image is based on many abrupt changes in the intensity level such as edge in an image.

Similarity detection based approach:

Similarity based approach based on partitioning a digital image into region those are similar to a predefined criteria. Histogram thresholding technique falls under the similarity detection based approach.

2 APPLICATION OF IMAGE SEGMENTATION

2.1 Medical imaging

- Define tumors and different pathologies
- Measure tissue volumes
- Surgery planning

2.2 Content based image recovery

2.3 Automatic traffic control system

2.4 Recognition Tasks

- Face detection
- Fingerprint recognition

3 TYPES OF IMAGE SEGMENTATION METHODS

Image segmentation currently become more important and though finding a proper segmentation technique is big research area. Thousand of segmentation methods has been proposed there is not a single method which is used for any type of image.

Therefore, depending on features of the digital image a particular segmentation method is used. There are various literatures in which described specific segmentation techniques.

The most popular techniques are used for image segmentation: edge detection based techniques, thresholding method, region based techniques, watershed based techniques, clustering based techniques, partial differential equation based and artificial neural network based techniques etc. All techniques are not to same with each other respect to the technique used by those for segmentation. In the literature many segmentation techniques have been proposed. These techniques can be divided into two categories- The first category is boundary detection based approaches, which is used to partition a digital image by finding out closed boundaries. The second category is the region based approaches, that group together pixels to be neighbors and with similar values and divided groups of pixels that have dissimilar value. The proposed method seen as region-based approach. There are different methods for region-based segmentation and mainly discuss graph-based approaches and active contour approaches. Methods in graph-based approaches usually represent an image as a graph $G = (V, E, W)$, with pixels as graph nodes V , and pixels within distance r (graph radius) are connected with a graph edge in E . Weight value $W(i, j)$ measures the similarity between pixels i and j .

The higher $W(i, j)$, the more similarity between pixels i, j . W can be computed using the location/illumination/texture information of pixels. The graph-based methods can be divided into several subcategories. For image segmentation global information is used by the first subcategories. For segmenting local information is used by the second subcategories such as minimum spanning tree (MST)- based segmentation methods [9], [16]–[19]. The third subcategory is Multiscale-based approaches [14], [20], [21]. After graph based approaches, we review active contour approaches [22]–[24].

3.1 Graph Cut-Based Methods

The main idea of graph cut-based methods is to partition graph $G = (V, E, W)$ into related component A_i such that $\cup A_i = V$ and $A_i \cap A_j = \emptyset$ component A_i by deleting the edges linking to these components. Graph cut-based technique try to divided image by optimizing many well-defined global objective functions. Wu and Leahy [8] proposed a cut between two related components as $\text{cut}(A, B) = \sum_{u \in A, v \in B} W(u, v)$. They proposed a method called minimum cut for digital image segmentation in such a way that the smallest $(K - 1)$ cuts among all customized cuts are selected and the corresponding edges are removed to create K -subgraph partitions. Wu and Leahy mention that the minimum cut criteria favorable the formation of several smaller segments containing only several isolated nodes, which result in oversegmentation. To overcome these drawbacks, Shi and Malik [16] proposed a new measure of aspiration between two components. Instead of viewing the total weights of the two partial connectors, they calculate the cost of the cut as a fraction of the total connection of all the edges in the graph. This new measurement called N_{cut} is defined as $N_{\text{cut}}(A, B) = \text{cut}(A, B) \frac{\text{assoc}(A, V)}{\text{cut}(A, B) + \text{assoc}(B, V)}$ where $\text{assoc}(A, V) = \sum_{u \in A, t \in V} W(u, t)$ is the total connections from nodes in A to all nodes in the graph and $\text{assoc}(B, V)$ is similarly defined. The main problem of segmenting a digital image to K regions is turned into problem of finding of the smallest $(K - 1)$ N_{cuts} . Graph cut-based methods usually give good segment results. However, they are time consuming. For example, for the N_{cut} method, Shi and Malik [26] showed that proper minimization of N_{cut} is NP-

hard. Therefore they proposed an approximation algorithm to solve a generalized eigenvalue problem having complexity $O(n^3)$, where n is denoted as number of pixels in a digital image. If the graph is sparse, e.g., each node (pixel) is the only neighbor's connection being inside a small graph radius r (e.g., $r < 10$), the complexity is reduced to $O(n^{3/2})$. Several works based on multiscale approach are proposed to accelerate Ncut [11]–[13].

3.2 Multiscale Graph Cut-Based Approaches

Sharon et al. [12], [13], at first, created a sparse graph, e.g., each pixel connects to its four nearest neighbors (NNs). To find the minimum Ncuts in the graph, they recursively uneven this graph using a weighted aggregation procedure in which they repeatedly selected smaller sets of representative pixels. The main goal of these coarsening steps is to produce small and small graphs which represent the same dispersion problem. Using this process, segments that are distinct from their environment will emerge and they are detected at their appropriate size scale. After construction of the entire pyramid and detect segments at different levels of the pyramid, they scanned this pyramid from top down performing relaxation sweeps to associate each and every pixels with appropriate segment. References [12] and [13] showed that the time usage of their algorithm is linear with the number of pixel of the image. Cour et al. [11] showed that if one increases number of neighbors in a node (e.g., increase graph radius r), a larger r generally makes the segmentation of Ncut better. However, increasing r also increases computation time. They also showed that can be divided into different scales of large radius graph and each of them contains connections with a special range of spatial separation. Hence, they adapted a multiscale approach for Ncut. In particular, given an image, they first downsample image at different scales $s \in \{1, \dots, S\}$. Let $Y_s \in \{0, 1\}^{N_s \times K}$ be the partitioning matrix at scale s ; N_s is the number of pixels at scale s , $N^* = \sum_{s=1}^S N_s$; $Y_s(i, k) = 1$ if graph node i belongs to partition k ; and $\mathbf{X} = [Y_1; \dots; Y_S] \in \mathbb{R}^{N^* \times K}$ is the whole multiscale partitioning matrix, then we can also rewrite \mathbf{X} by $\mathbf{X} = [X_1, \dots, X_1, \dots, X_K]$, where $X_l \in \{0, 1\}^{N^*}$ with $X_l(i) = 1$ where pixel i belongs to

segment l , W is the diagonal matrix where entries on the diagonal are weight matrices W_i , ($i = 1, \dots, S$) on scale levels, and D is a diagonal matrix where $D(m, m) = \sum_n W(m, n)$. The multiscale Ncut segmentation can be written as $\min_{\mathbf{X}} \sum_{l=1}^S \mathbf{X}^T l W X l \mathbf{X}^T l D X l$ s.t. $\mathbf{X} \in \{0, 1\}^{N^* \times K}$; $X_l K = \sum_{i=1}^{N^*} Y_{s+1}(i) = \sum_{j \in N_i} Y_s(j)$, $\forall s = 1, \dots, S-1$ where j (on scale s) $\in N_i$ is the sampling neighbor of i (on scale $s+1$) and the third constraint is to make the consistent segmentation across all the scales. This constraint means that the coarse-scale segmentation (Y_{s+1}) should be locally average of the fine-scale segmentation (Y_s). Using small graph radius (e.g., $r = 1$) at each scale, Cour et al. [11] showed that the running time of multiscale Ncut is $O(n)$, here n is total number of pixels in an image.

3.3 MST-Based Methods

Several methods in the MST-based approach model an image as an MST, and the segmentation is done by cutting the tree into several subtrees [16], [17]. The proposed methods in [9] and [18] do the segmentation in inverse way. At the beginning, each vertex is considered as the segment. Then, two segments are repeatedly selected to consider for merging in a greedy way. In particular, they defined that the difference between two segments is minimum weight connecting any two segments; the internal difference of a segment S is the largest edge of MST of S . Two segments will be merged if the difference between two segments is equal or less than to the minimum of the internal difference of the two segments. Felzenszwalb and Huttenlocher [9], [18] showed that their method can produce segments that are neither too fine nor too coarse. Because only local informations are used to decide if an MST should be split [16], [17] or if two segments of these should be merged [9], [18], MST-based methods are usually sensitive to noise. However, an advantage of these methods is that it is faster than graph cut-based methods [7]. For example, the most recent MST-based segmentation method proposed in [9] can run with the complexity $O(n \log n)$, where n is the number of image pixels. If the weights of edges are integer values (e.g., the difference in intensity of pixels), their algorithm can run in $O(n)$.

3.4 Multiscale-Based Methods

Multiscale-based segmentation works have been studied, including [12], [14], [20], and [21]. We have discussed a multiscale graph cut-based method in the previous part [27]. Arbelaez et al. [14] proposed a probabilistic boundary detection approach that combines both global and local information to detect boundary. Furthermore, they used a hierarchical segmentation approach to generate hierarchical segmentation regions. This method achieves state-of-the-art accuracy. Baatz and Schäpe [20] aimed to obtain high-quality segmentation results under different spatial scales. He combined both local and global optimization techniques, and used a scale parameter (SP) to control the average segment size in an image. He developed different similarity criteria to decide that whether or not to merge two objects in an image. Results showed that his segmentation approach can produce homogeneous image segments in an arbitrary scale. Agu t et al. [21] proposed an automated parameterization approach to decide the parameter SP in [38]. They used local variance (LV) information to select SP value. As LV value reached the optimal value, the corresponding SP value is selected. These two methods [20], [21] could generate good results on an image with geographical content.

3.5 Active Contour-Based Methods

The goal of active contour-based methods is to find the contours of objects in an image, by fitting active contours toward the object contours. There are some contour-based segmentation approaches that can achieve good results under some segmentation constraints. These constraints include interactive segmentation and segmentation on an image with relatively simple background. The method proposed in [22] used an active contour model to find out objects in an image. This model did not depend on the gradient of the image. Therefore, it could find out objects whose boundaries are defined by other information in addition to the gradient. This method could detect the object boundary properly when the background in the image is relatively simple and uniform. Lankton and Tannenbaum [23] proposed a model based on local information. They used a local region-based energy function rather than a global region-based energy function. By choosing a

good localization scale for an image, they can obtain accurate segmentations of the objects in an image. Nguyen et al. [24] proposed an interactive method based on continuous-domain convex active contour model. Their method showed robustness to user inputs and different initializations. Their method could produce smooth and accurate boundary contours with simple user inputs.

3.6 Fuzzy C-Means

The most widely used and more successful fuzzy clustering algorithm is the fuzzy c-means (MFC) which was proposed by Dunn in 1974 and generalized by Bezdek. According to the principle of the least square, iterative optimization is used for optimizing object function, and the final division of data is got after calculation. X is a parameter which is a kind of sample collection, and parameter n is represented the number of one sample collection. Parameter c indicated how many the feature can be divided, and that c centers will be used to cluster. Fuzzy C-means clustering algorithm is to divide a set with n elements into c small subsets. When it is applied to image segmentation, it means to divide the image into several different small areas according to the nature by the fuzzy clustering segmentation rules. Each area has no similarity by using clustering validity rule, the union set of each small area is the whole image area, and the result of fuzzy C - average clustering algorithm is to pick up the useful part of the classification.

Objective function of the fuzzy C - means clustering method is shown by the following:

$$1. J_m(U,V) = \sum_{i=1}^c \sum_j \mu_{ij}^m (X_j - V_i)^2$$

As we can see from the formula, it is clear that the fuzzy C-means division is a multi-dimensional matrix with $c \times n$. The image is segmented optimally by calculating the minimum value using formula (1). Update of the membership function and clustering center depends on the following two functions:

$$2. \mu_{ik} = \frac{1}{\sum_{k=1}^c (X_j - V_k) / (X_j - V_k)^{2/m-1}}$$

$$3. V_i = \sum_{k=1}^n (\mu_{ik})^m X_k / \sum_{k=1}^n (\mu_{ik})^m X^k$$

In each process of clustering, the degree of each pixel is calculated by Eq.2 for different center. The subjections degree with the largest class is where they belong to, which means clustering

center in each step has a different value. The subsection value with each step is different, the clustering results are also different.

3.7 Segmentation Based on Edge Detection

The grey level can be defined as the boundary between the two regions with specific characteristic. Edge detection can be defined as such a way that each object is surrounded by a closed border, which can be visible and the intensity of the image can be detect. It has very important role in pattern recognition and image analysis as it is described the physical extent of object.

Edge detection methods are following:

Roberts Edge Detection

For detecting edge, Roberts Edge detection technique is used. Lawrence Roberts was proposed this technique in 1963. This technique was first edge detector. The Roberts operator performs a simple, quick to compute, 2-D spatial gradient measurement on an image. It thus highlights regions of high spatial gradient which often correspond to edges. In its most common usage, the input to the operator is a grayscale image, as is the output. Pixel values at each point in the output represent the estimated absolute magnitude of the spatial gradient of the input image at that point. [4]

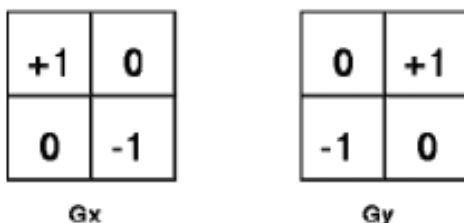


Fig. 1: Roberts cross convolution masks

Sobel Edge Detection

Sobel edge detector named after Irwin Sobel and it sometimes called as Sobel filter. Sobel edge detector is having two masks, one is vertical and other is horizontal. These masks are generally used 3*3 metrics. Standard Sobel operators, for a 3*3 neighborhood, each simple central gradient estimate is vector sum of a pair of orthogonal vectors [1]. Each orthogonal vector is a directional derivative estimate multiplied by a unit vector specifying the derivative's direction. The vector sum of these simple gradient estimates amounts to a vector sum of the 8

directional derivative vectors. Thus for a point on Cartesian grid and its eight neighbors having density values as shown:[2]

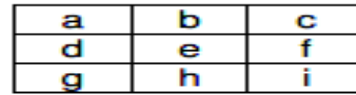


Fig. 2: Density values

Prewitt Edge Detection

Prewitt Edge Detector is used with edge detection algorithms in image processing. It is also called as Discrete Differentiation operator. It is used to calculate the gradient of the image intensity function. The Prewitt Edge filter is used to detect edges based applying a horizontal and vertical filter in sequence. Both filters are applied to the image and summed to form the final result. The two filters are basic convolution filters of the form: [3]

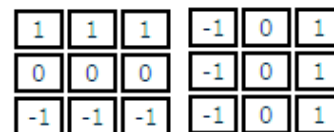


Fig. 3: Horizontal Filter Vertical Filter

3.8 Threshold Method

Threshold method is the mostly used technique in image segmentation. It is used to discriminate foreground from background. In this method, a grey scale image is converted into binary image [4]. The binary image contains the whole necessary data regarding location and shape of the objects. Conversion to binary image is useful because it reduces the complexity of data. Threshold methods are following:

Global Thresholding

In the global thresholding, the intensity value of the input image should have two peak values which correspond to the signals from background and objects. It tells the degree of intensity separation between two peaks in an image. Global thresholding, using an appropriate threshold T:

$$G(x, y) = 1, \text{ if } f(x, y) > T$$

$$= 0, \text{ if } f(x, y) \leq T \text{ [5]}$$

Variable Thresholding

In variable thresholding, we separate out the foreground image objects from the background based on the difference in pixel intensities of each region. Variable thresholding, if T can change over the image. Local or regional thresholding, if T depends on a neighborhood of (x, y) . Adaptive thresholding, if T is a function of (x, y) . [5]

Multiple Thresholding

Multiple thresholding can be defined as that segments a grey level image into several distinct regions. It defines more than one threshold for the given image and divides the image into certain brightness regions and it corresponds to the background and several objects. Multiple thresholding:

a, if $f(x, y) > T2$

$g(x,y) = b$, if $T1 < f(x, y) \leq T2$

c, if $f(x, y) \leq T$

3.9 Region Based Segmentation

Region Based segmentation can be defined as that in which we segment the similar image into various regions. It is used to determine the region directly. Partitioning is done by using grey values of the image pixels.[5]. Two basic techniques of region based segmentation are following:

Region Growing Method

Region growing is a technique that groups pixels or sub regions into larger regions based on predefined criteria. The pixels aggregation starts with a set of seed points in a way that the corresponding regions grow by appending to each seed points those neighboring pixels that have similar properties like grey scale, color, texture, shape etc.

Region Spitting and Merging

In case of region splitting, the whole image is taken as a single region and then this region is being break into a set of disjoint regions which are coherent with themselves. Region merging opposes Region Splitting. A merging technique is used after each split and compares adjacent regions and merges them. It starts with small regions and merge the regions which have similar characteristics like grayscale, variance etc.

3.10 Clustering Based Image Segmentation

Clustering based image segmentation is used to segment the images of grey level. Grey level methods can be directly apply and easily extendable to higher dimensional data. Clustering is also applicable in color and multispectral images. There are two main methods in clustering:

K-Means

The k-means methods of clustering are obtained based on the principle of minimization of the sum of squared distances from all points in each cluster domain to the cluster centre. This sum is also known as the within cluster as opposed to the between cluster distance which is the sum of distance between different cluster centre and the global mean of the entire data set. The objective of the algorithm is to minimize an objective function in order to assign a group of data to its centre [25].

Fuzzy K-Means

The Fuzzy K-means method is a two stage process involving a "coarse" segmentation followed by a "fine" segmentation. The "coarse" segmentation involves smoothing the histogram of each of the color components and using the first and second derivatives of the smoothed histograms to find the valleys which will then be the thresholds. A safe area surrounding the thresholds is then determined, and every pixel not falling into any safe area is assigned to a cluster based on its red, green and blue values and cluster centers are calculated. The "fine" segmentation involves assigning each pixel which belongs to a safe area to its closest cluster by calculating fuzzy membership functions.

4 CONCLUSION

Image segmentation is an important in the area of image processing and computer vision. In Image Segmentation an image is divided into multiple segments for analyzing the image. Different types of techniques and algorithms have been developed for image segmentation. The review of various image segmentation techniques, few methods on image segmentation have been studied and reviewed. FCM clustering

algorithm involves a lot of subjects, fuzzy mathematics is the theory basis of it, the construction of the model is quite flexible, the potential data of the image can be fully mined. None of the developed techniques has been developed universally for image segmentation. Since, new algorithms are being developed everyday to improve efficiency of segmentation. There are certain factors that affect the process of image segmentation like the intensity of image to be segmented, color, type and the noise present in the image. In medical images these can be used to detect cancer and in satellite images these can be used to detect roads and bridges. Thus it is clear that various methods are suitable for various types of image applications. But from the study it is clear that no single method is sufficient for every image type and no all methods are suitable for a particular image type. No algorithm has been developed till date that could keep a look at all the above listed factors and then segment the image effectively so that all the problems that can come in the way of image segmentation can be avoided. The algorithm development for effective image segmentation is still a big research that will take place in the area of image processing. Researchers still have to go a long way to develop efficient algorithm for image segmentation.

REFERENCES

- [1] W.X.Kang. Q.Q.Yang. R.R.Liang(2009)," The comparative Research on Image segmentation algorithm",IEEE conference on ETCS,pp 703-707.
- [2] SOBEL,I,An Isotropic 3X3 Gradient operator.Machine vision for three -Dimensional scenes,Freeman.H.,Academic Pres.NY,376-379,1990.
- [3] <http://www.roborealm.com/help/prewitt.php>
- [4] http://www.robotics.technion.ac.il/courses/advanced_laboratory/lab7/ar1_7_read.pdf
- [5] Stefano Ferrari university degli studi di Milano,"Image Segmentation",a.a.2011/12
- [6] N. R. Pal and S. K. Pal, "A review on image segmentation techniques," *Pattern Recognit.*, vol. 26, no. 9, pp. 1277–1294, Sep. 1993.
- [7] N. Ikonomakis, K. N. Plataniotis, and A. N. Venetsanopoulos, "Color image segmentation for multimedia applications," *J. Intell. Robot. Syst.*, vol. 28, no. 1, pp. 5–20, Jun. 2000.
- [8] E. Mendi, C. Yogurtcular, Y. Sezgin, and C. Bayrak, "Automatic mobile segmentation of dermoscopy images using density based and fuzzy c-means clustering," in *Proc. MeMeA*, Jun. 2014, pp. 1–6.
- [9] P. F. Felzenszwalb and D. P. Huttenlocher, "Efficient graph-based image segmentation," *Int. J. Comput. Vis.*, vol. 59, no. 2, pp. 167–181, Sep. 2004.
- [10] J. Shi and J. Malik, "Normalized cuts and image segmentation," *IEEE Trans. Pattern Anal. Mach. Intell.*, vol. 22, no. 8, pp. 888–905, Aug. 2000.
- [11] T. Cour, F. Benezit, and J. Shi, "Spectral segmentation with multiscale graph decomposition," in *Proc. CVPR*, Jun. 2005, pp. 1124–1131.
- [12] E. Sharon, A. Brandt, and R. Basri, "Fast multiscale image segmentation," in *Proc. CVPR*, Mar. 2000, pp. 70–77.
- [13] E. Sharon, A. Brandt, and R. Basri, "Segmentation and boundary detection using multiscale intensity measurements," in *Proc. CVPR*, 2001, pp. I-469–I-476.
- [14] P. Arbelaez, M. Maire, C. Fowlkes, and J. Malik, "Contour detection and hierarchical image segmentation," *IEEE Trans. Pattern Anal. Mach. Intell.*, vol. 33, no. 5, pp. 898–916, May 2011.
- [15] H. Zhang, J. E. Fritts, and S. A. Goldman, "Image segmentation evaluation: A survey of unsupervised methods," *Comput. Vis. Image Understand.*, vol. 110, no. 2, pp. 260–280, May 2008.
- [16] Y. Xu and E. C. Uberbacher, "2D image segmentation using minimum spanning trees," *Image Vis. Comput.*, vol. 15, no. 1, pp. 47–57, Jan. 1997.
- [17] Y. Xu, V. Olman, and E. C. Uberbacher, "A segmentation algorithm for noisy images: Design and evaluation," *Pattern Recognit. Lett.*, vol. 19, no. 13, pp. 1213–1224, Nov. 1998.
- [18] P. F. Felzenszwalb and D. P. Huttenlocher, "Image segmentation using local variation," in *Proc. CVPR*, Jun. 1998, pp. 98–104.
- [19] Y. Haxhimusa, A. Ion, W. G. Kropatsch, and T. Illieschko, "Evaluating minimum spanning tree based segmentation algorithms," in *Proc. 11th Int. Conf. CAIP*, 2005, pp. 579–586.
- [20] M. Baatz and A. Schäpe, "Multiresolution segmentation: An optimization approach for high quality multi-scale image segmentation," in *Proc. Angew. Geographische Informationsverarbeitung*, 2000, pp. 12–23.
- [21] L. Dr̃agu, t, O. Csillik, C. Eisank, and D. Tiede, "Automated parameterization for multi-scale image segmentation on multiple layers," *ISPRS J. Photogram. Remote Sens.*, vol. 88, pp. 119–127, Feb. 2014.
- [22] T. F. Chan and L. A. Vese, "Active contours without edges," *IEEE Trans. Image Process.*, vol. 10, no. 2, pp. 266–277, Feb. 2001.
- [23] S. Lankton and A. Tannenbaum, "Localizing region-based active contours," *IEEE Trans. Image Process.*, vol. 17, no. 11, pp. 2029–2039, Nov. 2008.
- [24] T. N. A. Nguyen, J. Cai, J. Zhang, and J. Zheng, "Robust interactive image segmentation using

- convex active contours," *IEEE Trans. Image Process.*, vol. 21, no. 8, pp. 3734–3743, Aug. 2012.
- [25] Siti Noraini Sulaiman, "Adaptive Fuzzy-K-Means clustering algorithm for Image Segmentation", IEEE.
- [26] D.L.Pham, c.Xu, and J.L.Prince (Aug, 2000) "Current Method in Medical Image Segmentation", *Annu.Rev.Biomed.Eng.*, Vol.2, pp315-337.
- [27] J.Bruce, T.Balch, and M.Veloso (2000), "Fast and inexpensive color image segmentation for interactive robots", in *proc.IROS*, Vol.3, pp.2061-2066.

Ms. Rozina Khatoon is an M.Tech Student at the Dept. of Computer Sc. & Engineering, Aliah University, Kolkata. She has done her B.Sc. in 2015 and M.Sc. in 2017 and pursuing M.Tech, all from Aliah University, Kolkata India.

Dr. Abhishek Das is currently working as the Head and Associate Professor in the Dept. of Computer Sc. & Engineering at Aliah University, Kolkata. His Research Area is in Medical Image Processing, Computer Vision and IoT. He has received a Post Doctoral Research position from University of West Scotland, UK by a Fellowship received from the European Commission. He has also worked as an Assistant Professor in the Dept. of Information Technology, Tripura University (A Central University), India. He has worked previously as a Reader in Computer Sc. & Engineering, Indian Institute of Space Science & Technology(IIST) and Lecturer in Information Technology, Bengal Engineering and Science University, Shibpur (now IEST Shibpur) His Ph.D is from the Dept. of Computer Sc. & Engineering, Jadavpur University, India. His M.S. in Electrical & Computer Engineering from Kansas State University, USA and B.Tech in Computer Science & Engineering from Kalyani University, India. He has worked as a Business System Analyst in Blue Cross Blue Shield New York, USA & as a Quality Analyst in Vensoft Inc. Phoenix, USA and also as a Consultant Project Manager in the Software Industry. He is also a Visiting Scientist at Indian Statistical Institute, Kolkata. He has also worked in Technical Educational Administration as Regional Officer and Asst. Director (on deputation) at AICTE (under MHRD, Govt. of India). He is a NCERT National Scholar, New Delhi and a Tilford Dow Scholar, USA. His Biography has been published in the 28th edition of National Dean's List, USA. He is a Member of IEEE and a Honorary Senior Member of IACSIT Singapore. He has several publications in International and National Journals and peer-reviewed Conferences. He is also a TPC Committee Member of IEEE International conferences in South-East Asia and Editor of the Journal of Image Processing and Pattern Recognition progress (A UGC recognised Journal) and Special Issues Journal on Image Processing & Computer Vision of IGI Global Publishers, USA (SCI and Scopus Indexed).

Noisy Gene Expression and Its Benefit

Rajesh Karmakar

Abstract—We are familiar with the term noise in electronic system and that has a detrimental role. Gene expression is a fundamental biological process whereby proteins are synthesized. Large numbers of experimental studies show that the gene expression is an inherently noisy process. We also know that the biological processes are fine-tuned and deterministic. Each and every processes of cellular system do happens at right moment. But noise generally destroys the tuning of such processes. In this work, we show that the noise in gene expression is not destructive rather has a benefit in cellular system.

Index Terms—Noise, Gene expression, Random switching, Stochastic simulation.



1 INTRODUCTION

GENE is a small part of DNA which stores the genetic information in the form of nucleotides (A, T, G, C etc.). Protein is a chain of amino acids with appropriate arrangement. They are prepared from a set of twenty amino acids and have distinct three-dimensional shapes. The genetic code or nucleotide sequence in the gene provides the blueprint for the synthesis of proteins. Proteins are the functional molecules in the cell. Different proteins do different jobs in the cell (e.g., mechanical support of the cell structure, transportation, manufacturer of other molecules and to the regulation of other proteins' activities or in defence against germs etc.). Gene expression is a process whereby proteins are produced according to the nucleotide sequence in the gene. Each gene carries the genetic information of one protein and each protein within the cell has a specific function [1].

Gene expression is a regulatory process and that plays the crucial role to achieve a perfect cellular system. A cell grows and divides perfectly from the embryonic stage to have a perfect structure and function of the body because of the accurate regulation of gene expression. This is mostly done by DNA binding proteins known as transcription factors (regulatory molecules) in eukaryotes (prokaryotes). Cell can control the amount of a protein it makes by regulating gene expression. Cells do not make all the proteins that their genome encodes continuously at high levels. Again, different kinds of cells contain identical sets of gene though all the genes do not produce all kind of proteins in the cell. For example, the gene synthesizing protein in hair cell remains inactive in blood cell. That is, under the regulation by transcription factor, gene can be either in the OFF or in the ON state in the cells.

Random switching takes place between two states. If the gene is in the ON state then only protein synthesis occurs with some specific rate. All the proteins have some specific half-life or degradation rate i.e., they do die after some time from the time of synthesis [1].

Gene expression and regulation is an important cellular process which ultimately controls the function and behaviour of every living system. So we expect that such fine-tuned biological process should evolve deterministically. Deterministic time evolution of protein synthesis gives a constant level of proteins at steady state. But scientists observed something different. In 2002, Elowitz et al. carried out an experiment at the single cell level and observed a fluctuating protein level about a steady value [2]. Such fluctuating level of proteins (Fig. 1) is pointed out as noise in gene expression [2]. We are habituated with the term noise in electronics which always has a harmful effect. In living system, the noise in protein level also has a harmful effect. The determinism in protein evolution is lost and the important processes may not remain fine-tuned due to noise. In general the protein level has to stay above a critical level for its proper functioning. But noise in protein level may bring down the protein level below the critical level thereby disrupting its function [3, 4]. There are many instances where the noise in gene expression produces harmful effects [5-8]. In spite of this detrimental role, the noise in gene expression may also have some beneficial role [9, 10, 11]. Micro organisms like bacteria have to cope with a multiple antagonistic agents and adverse environmental conditions in order to live. Under such situations, the bacteria may adopt a number of strategies to optimize their chances of survival. One such strategy is the development of genetic competence, observed in some bacterial organisms. In the competence state, some special proteins are synthesized which allow the cell to take up large pieces of DNA from the environment and incorporate them

• Dr. Rajesh Karmakar is Assistant Professor with the Department of Physics, Ramakrishna Mission Vidyamandira, Belur Math, Howrah, India. Email: rkarmakar@vidyamandira.ac.in

into the bacterial genome. New traits are thus acquired from genetically distinct organisms. Experiments show that only a small fraction of the bacterial population reaches the competence state. The resulting phenotypic diversity in the population due to noise in gene expression may prove to be beneficial. The individual cells in a homogeneous population share the same fate when subjected to harmful influences. Diversity enhances the chance that a fraction of the population, even if small, is able to survive and adapt to the changed circumstances. In *B. subtilis*, the development of competence is regulated by the transcription factor *ComK* synthesized by the *comK* gene. The protein functions as a master regulator which activates the transcription of several genes including those necessary for DNA uptake [9]. The noise in gene expression can be beneficial in changing environmental conditions. Increased variability in gene expression increases the adoptability under acute environmental stress [10, 11]. In this small seminal work, we show that noise in gene expression helps to stay above the critical level. We consider a simple model of gene regulatory network of two genes and show that the fluctuation in protein level from one gene helps to stay above the critical level of the proteins from other gene.

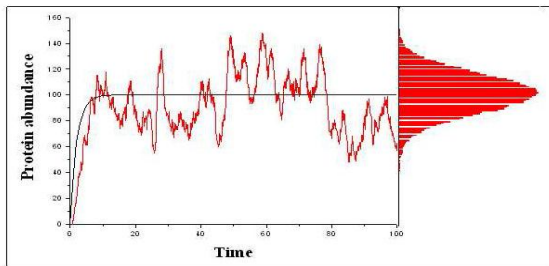


Fig. 1. Time evolution of protein's numbers (schematic) for deterministic (straight line) and noisy process (zigzag line). The distribution of protein's number is also shown (by stochastic simulation using GA).

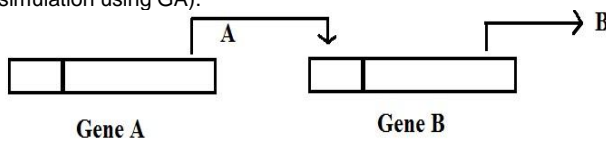


Fig. 2. Schematic diagram of two-gene network. Protein from gene A is regulating the synthesis of protein from gene B.

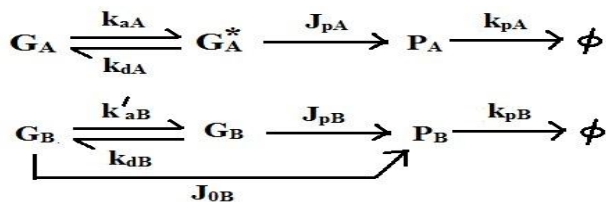


Fig. 3. Biochemical reactions and rate constants for the gene network. G_i (G_i^*) is the inactive (active) state of the ($i=A$ or B) gene. k_{ai} (k_{di}) is the activation (deactivation) rate constant. J_{pi} is the protein synthesis rate constant and k_{pi} being the degradation rate constant. J_{oB} is the basal rate of protein synthesis from inactive state of gene A. ϕ is the degradation product.

2 THE MODEL

We consider a network of two genes: Gene A and Gene B (Fig. 2). The protein from gene A is regulating the synthesis of protein from gene B [4]. That is, the proteins from gene A work as the transcription factor (TF) for the gene B. The fluctuating TF proteins are thus regulating the synthesis of proteins from gene B. Under the regulation of TF proteins, the gene B can be either in the ON or OFF state. If the gene B is in the ON (OFF) state then protein synthesis from gene B takes place with rate constants J_{PB} (J_{oB}). The proteins from gene B have a degradation rate K_{PB} . The synthesis of TFs from gene A is also a regulatory process and regulated by some other proteins. Therefore, the gene A can also be either in ON or OFF states. We consider that the rate of protein synthesis from the ON state of gene A is J_{PA} and the degradation rate is K_{PA} . We ignore the basal level synthesis from gene A to make our simulation little bit simpler. The biochemical reactions are shown in Fig. 3.

3 MODEL ANALYSIS BY STOCHASTIC SIMULATION

The fluctuating or noisy protein level from a gene is due to the stochastic nature of biochemical processes taking place inside the cell [12]. In gene expression, several biomolecules take part in several biochemical events. In most cases, the numbers of biomolecules present in the system are very small. A biochemical reaction occurs when the reactants collide with each other. For moles of reactants (i.e., molecule numbers of the order 1023) the biochemical reactions can be expressed by deterministic chemical rate equations. The implicit assumption underlying that formulation is that the concentration of the reactants varies both continuously and differentially. But in living system, in many instances, the biomolecules are present in a few copies per cell so that the associated biochemical reactions become infrequent and probabilistic [13, 14]. That is, the timing of the biochemical events is an outcome of chance processes [12]. In such situation, the concentration of the molecules is not the correct variables rather the number of molecules become more appropriate variable because the number of molecules changes by integer number in each biochemical reaction. To describe such system one needs the Master equation rather than the deterministic rate equation approach for the evolution of protein numbers [12]. The Master equation gives the time evolution of probability of

protein numbers. But the analytical solution of the Master equation is difficult in most cases. D T Gillespie prescribed a stochastic simulation algorithm known as Gillespie Algorithm (GA) which correctly gives the evolution of the numbers of molecules in a system of reacting biomolecules [13]. The GA gives the answer of two primary questions for time evolution of biomolecules: i) when will the next reaction occur? and ii) what type of reaction will it be? We do the stochastic simulation for our system of two-gene network with the biochemical reactions given in Fig. 3.

4 THE SIMULATION RESULT

We consider a network of two genes. Each gene has two states: inactive and active. Random transitions can take place between the states with rate constants shown in Fig. 3. The activation of gene B is occurred by several steps through the binding of the *A proteins* at the promoter site of gene B. This multistep binding process is approximated by a modulation function, known as the Hill function $F=(P_A/K)^n/(1+(P_A/K)^n)$ where P_A is the number of *A protein*, n is the Hill coefficient [4]. K is an equilibrium rate constant and at $P_A=K$, the Hill function F becomes half of its maximum value. The Hill coefficient determines how many *A protein* binds the promoter site of gene B to activate the protein synthesis. The modulated activation rate constant for the gene B is therefore given by $k'_{AB} = k_{AB} F$ where k_{AB} is the maximum value of activation rate constant from inactive to active state of gene B. We use the following values of the rate constants for two genes.

For gene A: $k_{aA} = 4.0$, $k_{dA} = 4.0$, $J_{pA}=4.0$, $k_{pA} = 1.0$. That gives the mean *A protein* number as $\langle P_A \rangle = 2$. The average number of regulatory molecules in the actual system also remains very low [7, 8]. For gene B: $k_{aB} = 8.0$, $k_{dB} = 4.0$, $J_{pB}=20.0$, $k_{pB} = 0.1$. We also choose $K=\langle P_A \rangle$ and $n=4$ to realize the fluctuation effect maximum [4]. The physical meaning of $n=4$ is that the minimum number of required *A proteins* to activate the gene B is 4. The initial state of the system is given by $G_A=1$, $G^*_A=0$, $P_A=0$, $G_B=1$, $G^*_B=0$, $P_B=0$.

Then we simulate the reactions with the help of GA and calculate the two stochastic variables: which reaction will occur and when will it occur?

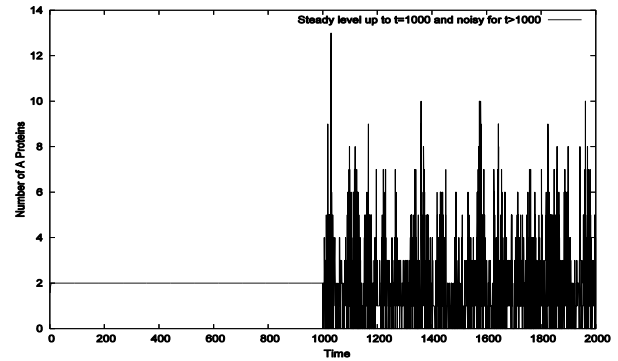


Fig. 4. Variation of numbers of *A proteins* with time. Steady level up to $t=1000$ and noisy expression of *proteins A* started at $t=1000$.

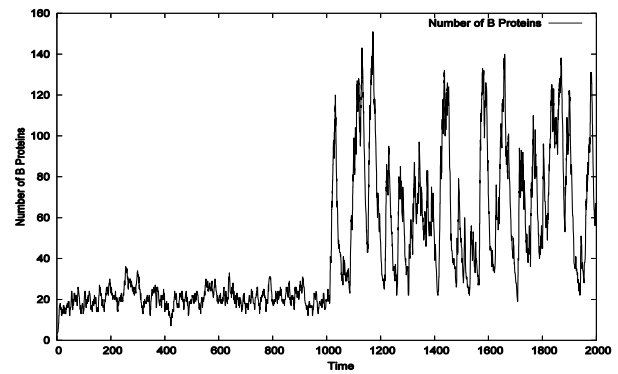


Fig. 5. Noisy expression level of *B proteins* with steady level of *A proteins* ($t<1000$) and noisy level of *A proteins* ($t>1000$)

In each step of simulation we then adjusted the state (number of different molecules) of the system and time. By repeated execution of the steps of GA we get the time evolution of molecular number. In Fig. 4, the time evolution of *protein A* is shown. In that figure, we have shown the steady behaviour of *A protein* up to $t=1000$ and beyond that the noisy expression started. In Fig. 5, we see that for the steady level of *A proteins* at the value 2 which is less than the Hill coefficient ($n=4$ here), the gene B fails to get activated by *A protein*. This results the expression of *B proteins* with low level ($\langle P_B \rangle = 20$). But, as the noisy protein expression (with the same mean value as in the deterministic case) from gene A started at $t=1000$, the *B proteins* started to express at high level with a mean value of 80. Though, we have shown the result here for only two sets of parameters values but the result will remain true for other values of rate constants also. Actually, the expression profile of a gene does not depend on the absolute value of the rate constants rather depends only on the relative values [16].

5 CONCLUSION

In this seminal work, we consider a network of two genes. The protein from one gene is regulating the protein synthesis from other gene. The experimental

evidences show that the gene expression process in cellular system is inherently noisy [2, 15, 16]. We are accustomed to the concept that noise is always harmful and steady value is beneficial. Noise in gene expression can have some benefits too [10, 11]. Here we see that steady value of the *A proteins* is not helpful to activate the protein synthesis from gene B whereas the noisy level in *A proteins* with the same steady or mean value is helpful to activate the gene expression from gene B. This is because, the instantaneous value of the *A proteins* sometimes getting higher than the threshold value (which is $n=4$ here) with the noise in *A proteins*. As the number of *A proteins* crossed the threshold value the gene B gets activated and starts to synthesis. It should be mentioned here that the amount of noise in *A proteins* should be sufficient to activate the gene B. In cellular system, proteins do some important job. To do so, protein level has to stay above a critical level. That is very important because protein level may become half due to genetic mutations in eukaryotic diploid system [4, 17]. So, the cellular system may use the noise to keep the protein level above the critical level in spite of the mutation. It should be mentioned here that the degradation rate of *B proteins* plays an important role to stay above the critical or threshold level. With lower degradation rate constant, the *B proteins* take more time to come down below the critical level.

In general, the noise in electronic systems has a detrimental role. But, in cellular system, we observed that the noise in protein level has a beneficial role. In this work, we have considered a network of two genes only. But in actual cellular system, the network can be a cascade of genes. The effect of gene expression noise in such network will be studied in future.

REFERENCES

- [1] B Alberts, A Johnson, J Lewis, M Raff, K Roberts and P Walters, Molecular Biology of the Cell, Garland Science, UK, 2002.
- [2] M B Elowitz, A J Levine, E D Siggia and P S Swain, Stochastic gene expression in single cell, Science vol. 297, pp. 1183-1186, 2002.
- [3] I Bose and R Karmakar, The biology of genetic dominance, Chapter 6, Landes Bioscience, Georgetown, 2004.
- [4] R Karmakar and I Bose, Stochastic model of transcription factor-regulated gene expression, Phys. Biol., Vol. 3, pp. 200-208, 2006.
- [5] D L Cook, A N Gerber and S J Tapscott, Stochastic gene expression: implications for haploinsufficiency, Proc. Natl Acad. Sci., vol. 95, pp. 15641-15647, 1998.
- [6] R A Veitia, Exploring the etiology of haploinsufficiency, Bioessays, vol. 24, pp. 175-184, 2002.
- [7] J G Seidman and C Seidman, Transcription factor haploinsufficiency: when half a loaf is not enough, J. Clin. Invest., vol. 109, pp. 451-455, 2002.
- [8] J A Magee, S A Abdulkadir and J Milbrandt, Haploinsufficiency at the *Nkx 3.1* locus. A paradigm for stochastic, dose-sensitive gene regulation during tumour initiation, Cancer Cell, vol. 3, pp. 273-83, 2003.
- [9] W K Smits, O P Kuipers and J W Veening, Phenotypic variation in bacteria: the role of feedback regulation, Nat. Rev. Microbiol., Vol. 4, pp. 259-271, 2006.
- [10] M Skipper, Benefits of noise, Nature Review Genetics, vol. 8, pp. 1, 2007.
- [11] W J Blake et al., Phenotypic consequences of promoter-mediated transcriptional noise, Mol. Cell, vol. 24, pp. 853-865, 2006.
- [12] N G van Kampen, Stochastic processes in physics and chemistry, North-Holland, Amsterdam, 1985.
- [13] D T Gillespie, Exact stochastic simulation of coupled chemical reactions. J. Phys. Chem., vol. 81, pp. 2340-2361, 1977.
- [14] M Karn, T C Elston, W J Blake and J J Collins, Stochasticity in gene expression: From theories to phenotypes, Nat. Rev. Gen., vol. 6, pp. 451-464, 2005.
- [15] J M Raser and E K O'Shea, Noise in gene expression: origin, consequences and control, Science, vol. 309, pp. 2010-2013, 2005.
- [16] R Karmakar and I Bose, Graded and binary responses in stochastic gene expression, Phys. Biol., Vol. 1, pp. 1-8, 2004.
- [17] R Fodde and R Smits, A matter of dosage, Science, vol. 298, pp. 761-763, 2002.

Dr. Rajesh Karmakar is Assistant Professor at the Department of Physics, Ramakrishna Mission Vidyamandira, Belur Math, Howrah. His research focuses on stochastic processes in Biology, nonlinear dynamics, nonequilibrium statistical mechanics, computational biology etc.

Face Detection and Eye Extraction using Canny Edge Detection and Hough Transform

Dildar Ali and Abhishek Das, *Member, IEEE*

Abstract—Presently days Face Detection and eye extraction is getting more consideration among researcher as it has an imperative job in numerous applications in science, for example, Facial appearance investigation, Security login and so forth. For a machine it is hard to detect human confront, distinctive facial structure like nose eye and so forth. This paper proposed a novel procedure for face recognition and eye extraction from a face picture utilizing vigilant Edge Detection and Hough Round Transform Algorithm for Circle fitting. It is seen that eye district of a picture are portrayed by low light, high-thickness edges, and high complexity as compared to different parts of the face. The proposed moved toward methodology is partitioned into two primary advances. Firstly, Face district recognizable proof is finished utilizing watchful Edge identification and besides, Eyes are extracted from the face locale with the assistance of Hough transformation and Circle fitting Algorithm.

Index Terms—Canny Edge Detection, Hough Round Transform, Circle Fitting Algorithm, Face Detection, Eye Detection

1 INTRODUCTION

HUMAN face recognition, analysis, detection is an important application of pattern recognition. This is become currently one of the important research topic in the field of computer vision. The eye is most significant and important feature in human face. Detection of eye is a crucial aspect in many useful applications ranging from face recognition and face detection to human computer interface design model based video coding, driver behavior analysis, compression techniques development and automatic annotation for image databases etc [11]. A large number of materials proposing various techniques have been published on this subject in the last couple of decades but the effectiveness of these techniques have not been satisfactory enough due to the complexity of the problem. Given the benefits of this aspect in a multitude of areas, a solution to this problem has to be found. Generally, the detection of eyes is done in two phases: locating the face to extract eye regions [8] and then extract the eyes from these regions [9], [12]. In this paper face and eyes are recognized by edge detection strategy and Hough round change from an image which contains a single human face. Section 2 depicts related work of face location and Eyes extraction. The proposed work is introduced in section 3 and section 4 concludes the proposed work.

- Dildar Ali is a M.Tech Student with the Dept. of Computer Science and Engineering, Aliah University, Kolkata, India. Email: dildarskp1994@gmail.com
- Dr. Abhishek Das is Associate Professor and Head with the Dept. of Computer Science and Engineering, Aliah University, Kolkata, India Email: adas@aliah.ac.in

2 Related Work

Here we can use many techniques positioning detection, including the region segmentation method, edge extraction, gray projection method and template matching method. The main eye location algorithm: Zhou used generalization projection function method [1].

Reinder used method is neural networks and micro-properties of the eye to locate the human face features [2].

Zhu proposed used the integral image to find the candidate point and then make use of SVM verify the result [3].

Kawaguchi and Rizon an algorithm eyes were extracted by intensity value from face region using edge detection, Different morphological operations, region growing algorithm and Hough circle transformation [4]. The drawback of this approach is slow computation.

Viola and Jones used integrated image, AdaBoost learning algorithm with some features and combining the classifiers in cascade face detection [5]. The drawback of this approach is slow learning method and large no of features.

Shafi and Chung also proposed edge density based method for frontal face image using histogram equalization, morphological

operations and sobel edge detection [6]. In this approach different size image may did not work properly due to the size of structuring elements.

$$|G| = \sqrt{G_x^2 + G_y^2} \quad (1)$$

A. Singh, M. Singh and B. Singh proposed face detection and eyes extraction using sobel edge detection and morphological operations [7].

From the survey, it is observed that the vast majority of the algorithms are computationally costly. Thus, it further gives a degree to enhance the precision and also least computational multifaceted nature. Considering this methodology that proposed for face recognition and eye extraction from single face picture, this calculation depends on Canny edge detection and Hough round circle transformation.

2.1 Canny edge detection

The Canny edge detection algorithm is known to many as the optimal edge detector. Canny's ideas and methods can be found in a paper, "A Computational Approach to Edge Detection" [15]. In this paper, the first and most obvious success is low error rate. It is important that edges occurring in images should not be missed and that there be no responses to non-edges. The second criterion is that the every edge points be well localized.

Based on these criteria, the canny edge detector first smoothes the image to eliminate the noise. It then finds the image gradient to highlight regions with high spatial derivatives.

$$G_x = (I * g_x) \quad (2)$$

$$G_y = (I * g_y) \quad (3)$$

The edge strength G ,

$$G = \sqrt{G_x^2 + G_y^2} \quad (4)$$

Edge detection is defined as the direction of tangent to the contour of that edge defines by a two dimensional image.

$$A = \arctan(G_x / G_y). \quad (5)$$

The algorithm then tracks along these regions and apply non maximum suppression. The gradient array is further reduced by hysteresis. Hysteresis is used to track along the remaining pixels that have not been suppressed. Hysteresis uses two thresholds and if the magnitude is below the first threshold, it is set to zero. If the magnitude is above the high threshold, it is made an edge. And if the magnitude is between two thresholds, then it is set to zero unless there is a path from this pixel to a pixel with a gradient above second threshold.

2.2 Hough Transform

The Hough transform method can be used to find features of any shape in an image. In practice it is only used for finding straight lines or circles. The computational complexity of the method grows rapidly with shapes that are more complex. Consider a point (x_i, y_i) in the image [14]. The general equation of a line is

$$y = ax + b \quad (6)$$

There are infinitely many lines that pass through this point, but they all satisfy the condition

$$y_i = ax_i + b \quad (7)$$

for varying a and b .

Rewriting this equation as

$$b = -x_i a + y_i \quad (8)$$

and plot the variation of a and b .

By divide parameter space into a number of discrete accumulator cells we can collect 'votes' in $a b$ space from each data point in $x y$ space. Peaks in $a b$ space will mark the equations of lines of co-linear points in $x y$ space.

However, there is a problem with using $y = ax + b$ to represent lines when the line is vertical. In that case $a = \infty$ and the parameter space is unbounded.

An alternative representation of a line is given by $x \cos \theta + y \sin \theta = r$ (9)

Where r is the distance of the line from the origin and θ is the angle between this perpendicular and the x-axis. Our parameter space is now in θ and r , where, $0 \leq \theta \leq 2\pi$ and r is limited by the size of the image.

As before, peaks in the accumulator array mark the equations of significant lines.

In theory any kind of curve can be detected if express it as a function of the form

$$f(a_1, a_2, a_3, \dots, a_n, x, y) = 0 \quad (10)$$

For example, a circle can be represented as

$$(x - a)^2 + (y - b)^2 - r^2 = 0 \quad (11)$$

One then has to work in n dimensional parameter space (three-dimensional space for a circle).

This model has three parameters: two parameters for the centre of the circle and one parameter for the radius of the circle. If the gradient angle for the edges is available, then this provides a constraint that reduces the number of degrees of freedom and hence the required size of the parameter space [10]. The direction of the vector from the centre of the circle to each edge point is determined by the gradient angle, leaving the value of the radius as the only unknown parameter.

$$x = a + r \cos \theta \quad (12)$$

and

$$y = b + r \sin\theta \quad (13)$$

Solving for the parameters of the circle we obtain the equations

$$a = x - r \cos\theta \quad (14)$$

and

$$b = y - r \sin\theta \quad (15)$$

Now using the gradient angle θ at an edge point (x,y) , easily compute $\cos\theta$ and $\sin\theta$.

2.3 Circle Fitting Algorithm

- 1 Quantize the parameter space for the parameters a and b .
- 2 Zero the accumulator array $M(a,b)$.
- 3 Compute the gradient magnitude $G(x,y)$ and angle $\theta(x,y)$.
- 4 For each edge point in $G(x,y)$, increment all points in the accumulator array $M(a,b)$ along the line
 $b = a \tan\theta - x \tan\theta + y \quad (16)$
- 5 Local maxima in the accumulator array correspond to centres of circles in the image.

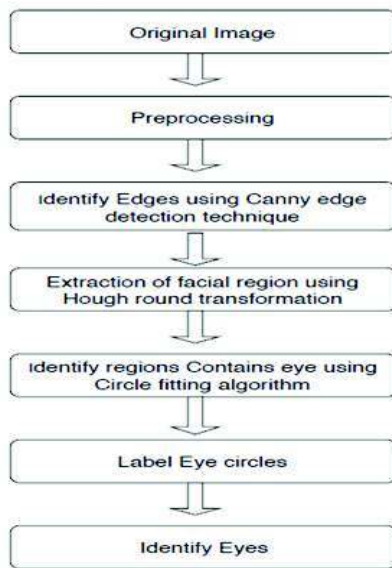


Fig. 1. Flow chart for Eye Identification

3 PROPOSED WORK

In this paper, it proposed a method in three steps preprocessing, Face detection, Extraction of eyes. The steps are in given fig. 1.

3.1 Preprocessing

The shading picture is changed over into grayscale picture as appeared in fig. 2. As the edge recognition strategy is relies upon gray scale image, gray scale color image is taken as color space model [7].



Fig. 2. Gray scale image

3.2 Identify Facial region

Eye detection technique is applied to grey scale image to find edges in order to separate foreground and background. Eye detection makes sharp edges and back ground of the image in black region as there intensity variation is high [14]. The Canny edge detection technique is used to the image as shown in fig.3 [15].



Fig. 3. Edge detection

3.3 Eye Extraction

This labeling system is designed for specific Portrait images, it work best with a plain background. This Method is trying to label the eyes Using a Simple Parameters and Correlations between the circles [13]. It tries to find the best match, two circles that suit the eyes [14]. The given methods used to give points to circles and to filter circles.

1. The Slope between the circles.

As here used a portrait images it assumed the head or eyes are having a slope of less than 45 degrees. It checks for each circle if got a friend Circle with that slope. If no then again filter.

2. The Distance between two Circles.

Distance is not too Close or not too Far in each 2 circles, if it found an isolated circle that have friend too far (width /2), because of assuming all the face is inside the image.

3. Number of circles in the area of the circle.

It is observed during testing with the Hough circle that the area of the eyes gives many circles

in the same place or very close, so an approach points to circles that are congruent Depending on the number of circles is used.

4. The Radius compatibility between the circles

The last method is checking the circle radius, if the radius size is closer or even compatible it might get more points. The reason is obvious the eyes are in the same size and probably the circles of the eyes are pretty much the same size.



Fig. 4(a). Eye Detection



Fig. 4(b). Resultant Image

4 CONCLUSION

This paper proposed a technique for eye detection using Canny edge detection technique and Hough round transform. It is observed after testing 6 Images that out of 6 images: 5 has given good results. That is meaning that approximately the success is 83%. However, this technique needs to be improved for two or more faces in an image is used. The current code is written in MATLAB (R2016a) and compilation time is 10-12 seconds of run time in 2GHz processor. Therefore, the Program is good enough to detect eyes for a single face image.

REFERENCES

- [1] Zhou Z. H. Geng X. Projection functions for eye detection [J]. Pattern Recognition, 2004; 37(5): 1049-1056.
- [2] Reinders M, Koch R, Gerbrands J. Locating facial features in image sequences using neural networks. FG, 1996: 230-235.
- [3] Zhu Z W, Fujimura K K, Ji Q. Real-time eye detection and tracking under various light conditions [C]. Proceedings of ACM SIGCHI Symposium on Eye Tracking Research and Application, New Orleans, LA USA, 2002: 139-144.
- [4] T. Kawaguchi and M. Rizon, "Iris detection using intensity and edge information", pattern Recognition, vol 36(2), pp. 549-562, 2003.
- [5] P. Viola and M. J Jones, "Robust real time face detection", International Journal of Computer Vision, vol 57(2), pp. 137-154, 2004.

- [6] M. Shafi and P.W.H Chung, "Eye extraction from facial images using edge density", 7th IEEE International Conference on Cybernetic Intelligent Systems (CIS), pp. 1-6, 2008.
- [7] A. Singh, M. Singh and B. Singh, "Face detection and eyes extraction using sobel edge detection and morphological operations," 2016 Conference on Advances in Signal Processing (CASP), Pune, 2016, pp. 295-300.
- [8] M. Ashwini, N. Chakravarty, N. M, R. R. Gaikwad, and M. A N, "Eye Detection in frontal face images", International Research Journal of Engineering and Technology, vol. 1(2), pp. 1-10, 2013.
- [9] T. Rajpathak, R. Kumar, and E. Schwartz, "Eye detection using morphological and color image processing," Proceeding of Florida Conference on Recent Advances in Robotics, pp. 1-6, 2009.
- [10] Y. Ito, W. Ohyama, T. Wakabayashi, and F. Kimura, "Detection of Eyes By Circular Hough transform and histogram of gradient", 21st IEEE International Conference on Pattern Recognition, pp. 1795-1798, 2012.
- [11] S. Rani, D. Bansal, and B. Kaur, "Detection of edges using mathematical morphological operators", open Transactions on Information processing, vol, 1(1), pp. 17-26, 2014.
- [12] J. A Nasari, S. Khanchi, and H. R. Pourreza, " Eye Detection Algorithm on facial Color Images," in Modeling & Simulation, 2008, pp. 344-349.
- [13] O. F. Soylemez and B. Ergen, " Circular hough transform based eye state detection in human face images," in Signal Processing and Communications Applications Conference (SIU), 2013 21st, 2013, pp. 1-4.
- [14] Deepika Rani Sona, Prayline Rajabai. C, Debopam Dey, Akansha Jain, Rashmi Ranjan Das and Stephen Olatunde Olabiyisi, A case Study: Edge Detection Technique Using Hough Transform and Canny Edge Algorithm, International Journal of Mechanical Engineering and Technology 8(10), 2017, pp. 729-740.
- [15] J. Canny, "A Computational Approach to Edge Detection," in IEEE Transactions on Pattern Analysis and Machine Intelligence, vol. PAMI-8, no. 6, pp. 679-698, Nov. 1986.

Dildar Ali is currently pursuing M.Tech in Computer Science and Engineering from Aliah University, Kolkata, India. He obtained his 5-years integrated Master of Computer Application from Aliah University, Kolkata in 2018. His research interest areas are Image Processing, Machine Learning and Data Science.

Dr. Abhishek Das is currently working as the Head and Associate Professor in the Dept. of Computer Sc. & Engineering at Aliah University, Kolkata. His Research Area is in Medical Image Processing, Computer Vision, Machine Learning and IoT. He has received a Post Doctoral Research position from University of West Scotland, UK and Ph.D is

from the Dept. of Computer Sc. & Engineering, Jadavpur University, India. His M.S. in Electrical & Computer Engineering from Kansas State University, USA He is a NCERT National Scholar, New Delhi and a Tilford Dow Scholar, USA. His Biography has been published in the 28th edition of National Dean's List, USA. He is a Member of IEEE and a Honorary Senior Member of IACSIT Singapore. He has several publications in International and National Journals and peer-reviewed Conferences. He is also a TPC Committee Member of IEEE International conferences in South-East Asia and Editor of the Journal of Image Processing and Pattern Recognition progress(A UGC approved Journal) and Special Issues Journal on Image Processing & Computer Vision of IGI Global Publishers, USA (SCI and Scopus Indexed).

Study on Supercontinuum in Dispersion Engineered Silicon Nanowire

Ranjit Das

Abstract—A fine-tuned dispersion engineered structure of a silicon nanowire is reported here for producing an efficient supercontinuum optical source. Employing full-vectorial finite element method, efficient supercontinuum of 600 nm bandwidth at pump power 50 W is generated in dispersion engineered Silicon nanowire. Effects of propagation loss, two photon absorption, free carrier absorption and geometrical parameters of the nanowire are also addressed in this report.

Index Terms—Dispersion engineering, Nonlinear optics, Silicon nanowire, Supercontinuum

1 INTRODUCTION

SUPERCONTINUUM (SC) source can provide smooth spectrum of large bandwidth, high brightness and increased spatial coherence [1,2]. Generation of SC depends on various nonlinear phenomena in the guiding medium such as self-phase modulation (SPM) [3,4], cross-phase modulation (XPM) [5], soliton dynamics [6], Raman scattering [7] and four wave mixing (FWM) [8]. Many approaches have been reported for SC generation, such as, using silica waveguides [9], single mode fibers [1], photonic crystal fibers [10] and LiNbO₃ waveguides [11]. Nowadays Silicon-On-Insulator (SOI) is very prospective due to its high Kerr nonlinearity, Raman amplification, self-phase modulation, four wave mixing, soliton formation [2,6,8,12] and good transparency in the communication bands. Large index contrast between core and cladding in Silicon nanowire results in high light confinement in the sub-micron waveguide. High light confinement results in large effective nonlinearities in the guiding media causing further broadening of the SC [2,12]. Nonlinear effects such as two-photon absorption (TPA), free carrier absorption (FCA), free carrier dispersion (FCD), modulation instability (MI) and Cherenkov radiation have great impact on SC generation [1,2,4,12].

Although Silicon has low losses in near infrared, it has some disadvantages in the communication band centered at 1550 nm where both TPA and FCA clamp the SC spectra [3]. As reported in [13],

SC broadening is increased when the pump wavelength is chosen close to the Zero Dispersion Wavelength (ZDW). This is due to the reduced linear dispersion resulting in smaller temporal pulse broadening and causing strong nonlinear interaction. Also it reports that the broadening of SC saturates for relatively high pump power due to the influence of TPA. But in the present work a further broadening of SC is reported by employing pump with higher input power. The work reported here is basically to find the fine-tuned air-clad Silicon nanowire structure so that the SC spectra can be broadened further at 1550 nm.

2 THEORY

First, the effective dispersion of the nanowire is calculated by employing the Sellmeier equations of the waveguide materials and provided as input to the FEM to obtain the wavelength and geometry dependent effective index. The effective indices obtained from the Finite Element Method (FEM) are used to extract the Group Velocity Dispersion (GVD) of the nanowire. Then the optimized dimension of the nanowire is obtained for which the desired pump wavelength is just greater than the lower ZDW. To enable excitation only of the fundamental quasi-TE mode in the waveguide its height is chosen to be 220 nm [14].

To study SC generation, simulations were performed using a generalized nonlinear Schrödinger equation (GNLSE) for the slowly varying envelope of the pulse [4,6]:

• Ranjit Das is with the Department of Computer Science and Electronics, Ramakrishna Mission Vidyamandira, Belurmath, Howrah, West Bengal, INDIA, 711 202. E-mail: ranjitdas.in@gmail.com, ranjitdas@vidyamandira.ac.in.

$$\begin{aligned} \frac{\partial}{\partial z} A(z, T) = & -\frac{\alpha_l + \alpha_f}{2} A + \sum_{r \geq 2} \frac{i^{r+1}}{r!} \beta_r \frac{\partial^r A}{\partial T^r} \\ & + i \left(\gamma + i \frac{\alpha_2}{2A_{\text{eff}}} \right) \left(1 + \frac{i}{\omega_0} \frac{\partial}{\partial T} \right) \\ & \times \left(A(z, T) \int_{-\infty}^{\infty} R(T) |A(z, T - t')|^2 dt' \right), \end{aligned} \quad (1)$$

Here, A is the electric field amplitude, α_l is the linear propagation loss, α_f is the loss associated with FCA, $\beta_r(\omega) = (d^r \beta / d\omega^r)|_{\omega=\omega_0}$, ($r \geq 2$) is the r^{th} dispersion parameter, and $T = t - z/v_g$ is the retarded time frame moving with the group velocity $v_g = [\beta_1(\omega_0)]^{-1}$. The nonlinear coefficient is $\gamma = n_2 \omega_0 / [c A_{\text{eff}}(\omega_0)]$, where n_2 is the nonlinear refractive index and c is the speed of light in vacuum, $A_{\text{eff}}(\omega_0)$ is the effective area of the mode at ω_0 , and $\alpha_2 = 5 \times 10^{-12}$ m/W is the TPA coefficient [4]. Also $\alpha_l = 3.6$ dB/cm [13] and $n_2 = 6 \times 10^{-18}$ m²/W [4]. Here α_f is negligible as it has very small influence on the soliton propagation [6,13]. The material response function, $R(t)$ includes both the instantaneous electronic response of Kerr type and the delayed Raman response.

Generally, a secant pulse represented by the following equation is used to excite the waveguide for SC generation [6], $A(t) = \sqrt{P_0} \cdot \text{sech}(t/T_0)$. The secant pulse with desired features is fed through the silicon nanowire of optimized geometry, designed on SOI, schematic of which is shown in Inset (i) of Fig. 1(a).

3 NUMERICAL STUDY AND RESULTS

GVD parameters of the nanowire over entire wavelength range are calculated from the effective indices obtained from the FEM considering mesh size of 800×800 . Optimized dimension (770×220 nm²) of the nanowire is then achieved by analyzing the GVD plots [Fig. 1(a)] for various geometries of the nanowire at pump wavelength 1550 nm.

The present study is based on the time domain evolution of the SC using a split-step Fourier method. Higher order dispersion terms β_r upto 10th order were evaluated from the dispersion curve shown in Fig. 1(a). It is expected that the extent of the SC depends on the higher order dispersion terms. In that case sufficient number of terms needs to be included in Eq. (1). To study

the effect of higher order β , first a data fitting technique based on Taylor series expansion is considered to find the highest order number of β which may be sufficient to replicate the original GVD curve [Fig. 1(b)]. Here, it can be concluded that terms upto β_{10} is sufficient for exact representation of the generated SC.

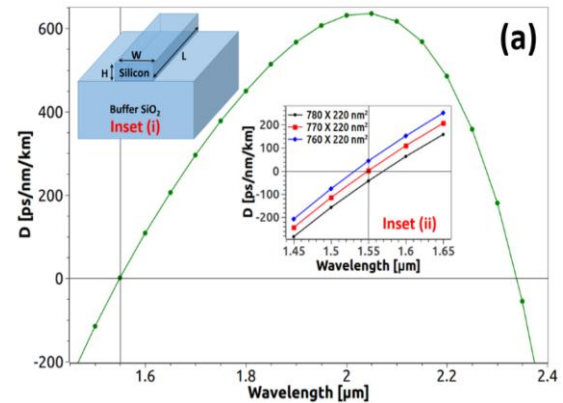


Fig. 1. (a) GVD of the fundamental quasi-TE mode for an optimized Si nanowire of cross-section 770×220 nm², Inset (i) shows the schematic of the nanowire & Inset (ii) shows the effect of nanowire width on the GVD.

Next, effect of higher-order dispersion terms on the SC bandwidth and flatness is examined. Hence Eq. (1) is employed to simulate the SC using MATLAB R2016a. Using the FEM, the effective mode area of the waveguide is obtained ($A_{\text{eff}} = 0.3158$ μm²) for the Si nanowire of optimized dimension at the pump of $\lambda = 1550$ nm, and hence the nonlinear coefficient (γ) is determined. To excite the nanowire a TE polarized secant pulse of 50 fs FWHM and peak power of 25 W, is launched inside it. In this simulation the value of propagation loss is chosen to be independent of the operating wavelength and is equal to 3.6 dB/cm [13]. The active length of the nanowire is taken as $L = 10$ mm. Negligible influence in the SC spectrum is noted for inclusion of higher order β_r for $r \geq 4$. This is in accordance with the fact that the supercontinuum of acceptable strength ranges approximately between 1400 – 1800 nm. In this range the higher order β 's do not show any visible influence on the GVD of the nanowire as shown in Fig. 1(b). To analyze the features of the generated spectra from the nanowire temporal

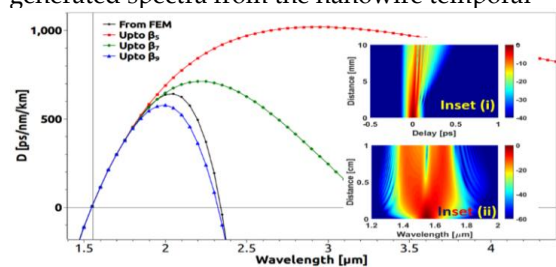


Fig. 1. (b) Dispersion curve obtained from FEM & Taylor series fitted curves upto the terms β_n ; temporal intensity [Inset (i)] & spectral density [Inset (ii)] of the SC corresponding to the inclusion of terms upto β_{10} .

intensity and spectral density corresponding to β_{10} are shown in the inset of Fig. 1(b). The pump being in the anomalous GVD regime, the generated SC is primarily dominated by the soliton fission process due to the interplay between SPM and dispersion of the nanowire.

With the said nanowire structure, the soliton order is $\bar{N} \approx 14$, and the soliton fission occurs at a distance of $L_{fiss} \approx 7.2$ mm when a pump of 25 W is employed. This is mainly due to the perturbation induced by third and higher order dispersion terms. It can be seen that multiple fundamental solitons are generated after the fission, which results in a shift of the spectra toward the longer wavelength side. Hence multiple spectral peaks in the stoke-side of the spectrum is resulted due to intrapulse Raman scattering. Again, spreading of the spectrum in the shorter wavelength (anti-stoke) region is associated with Non-Solitonic Radiation (NSR) in the form of dispersive wave. In general, the spreading of the SC in both sides of the pump wavelength depends strongly on how many dispersion terms are included, but for Si nanowires extension of the spectra on both sides is restricted by huge propagation loss in the shorter wavelengths and by TPA and FCA loss in the longer wavelengths.

The SC spectral bandwidth also depends on the pump power, which is illustrated in Fig. 2(a). It can be observed that the bandwidth corresponding to the 30 dBm spectral power increases with the pump power, e.g., it increases from approximately 400 nm for a pump power of 25 W to about 900 nm at 500 W. This is in contradiction with [13],

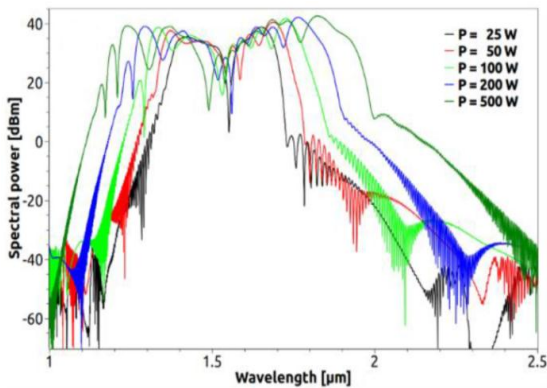


Fig. 2. (a) SC corresponding to different pump powers.

which states that SC broadening saturates for very high pump power (> 25 W) in Si nanowire. This may be associated to the high free carrier dispersion due to large free carriers generated

through TPA effect for very high pump power [4].

SC spectra with TPA effect (with/without FCA) are shown by a solid green line and a dashed black line, respectively, in Fig. 2(b,c). It is observed from these curves that FCA has insignificant effect on the SC for low and high

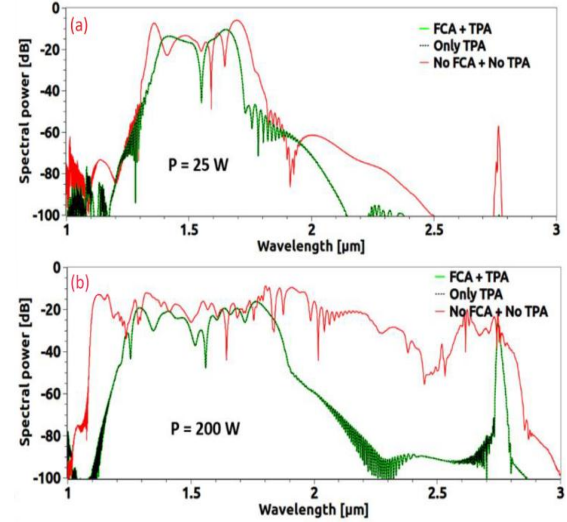


Fig. 2. Effect of TPA & FCA on the SC for pump power (b) of 25 W & (c) of 200 W, respectively.

pump powers, which agrees very well with literature [4,6]. But TPA has a considerable impact on the bandwidth of the SC which clamps the upper frequencies of the SC spectra. It can be seen for a hypothetical case when no TPA and FCA effects are present in a Si nanowire, the bandwidth can reach a larger extension.

Finally, a hypothetical study is made to understand the influence of high propagation loss of Si, high TPA and high FCA loss on the spectral broadening. In a lossless optimized Si nanowire of length 10 mm with zero TPA and zero FCA loss a -30 dB bandwidth of more than 600 nm is obtained for a pump of power 25 W [Fig. 2(d)]. In practice the SC bandwidth is

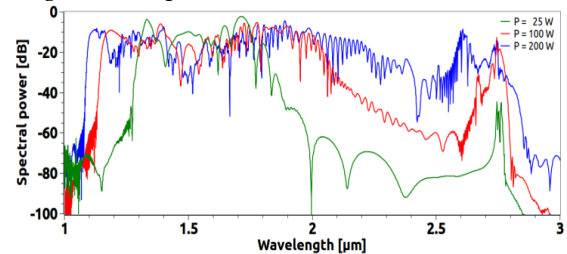


Fig. 2.(d) Effect of zero TPA & zero FCA loss on SC spectral width in hypothetical lossless Si nanowire of dimension 770×220 nm².

reduced due to high values of the loss parameters. Further broadening of SC spectra is

not possible with only Si nanowire structures having silica or polymer cladding, because use of these cladding materials will result in lesser index contrast as well as in lesser confinement inside the core. As a result, the nonlinear interaction will be reduced and the bandwidth will be shortened.

4 CONCLUSION

Using FE mode solver Si-nanowire of optimized dimension, $770 \times 220 \text{ nm}^2$, is obtained. It is observed that SC bandwidth can be increased with high pump power but this may create instability of the SC. High light confinement in Si nanowire creates large effective nonlinearities in the guiding media and results in broadening of the SC spectra. In this work it is observed that the combined effect of TPA and FCA clamps the spectral broadening of SC and limit the achievable bandwidth. Although a SC of bandwidth of approximately 900 nm at -30 dB is achieved, at pump power 500 W. Also, in a lossless Si nanowire a -30 dB bandwidth of more than 600 nm is obtained at 25 W.

REFERENCES

- [1] R. A. Soref, "The past, present, and future of silicon photonics," *IEEE JSTQE*, vol. 12, no. 6, pp. 1678–1687, Nov-Dec. 2006.
- [2] Q. Lin, O. J. Painter, and G. P. Agrawal, "Nonlinear optical phenomena in silicon waveguides: modeling and applications," *Opt. Exp.*, vol. 15, no. 25, pp. 16604–16644, Dec. 2007.
- [3] I. W. Hsieh, X. G. Chen, J. I. Dadap, N. C. Panoiu, and R. M. Osgood, Jr., "Ultrafast-pulse self-phase modulation and third-order dispersion in Si photonic wire-waveguides," *Opt. Exp.*, vol. 14, no. 25, pp. 12380–12387, Dec. 2006.
- [4] L. Yin, and G. P. Agrawal, "Impact of two-photon absorption on self-phase modulation in silicon waveguides," *Opt. Lett.*, vol. 32, no. 14, pp. 2031–2033, Jul. 2007.
- [5] G. Genty, M. Lehtonen, and H. Ludvigsen, "Effect of cross-phase modulation on supercontinuum generated in microstructured fibers with sub-30 fs pulses," *Opt. Exp.*, vol. 12, no. 19, pp. 4614–4624, Sep. 2004.
- [6] L. Yin, Q. Lin, and G. P. Agrawal, "Soliton fission and supercontinuum generation in silicon waveguides," *Opt. Lett.* vol. 32, no. 4, pp. 391–393, Feb. 2007.
- [7] K. J. Blow, and D. Wood, "Theoretical description of transient stimulated Raman scattering in optical fibers," *IEEE JQE*, vol. 25, no. 12, pp. 2665–2673, Dec. 1989.
- [8] L. Shen, N. Healy, L. Xu, H. Y. Cheng, T. D. Day, J. H. V. Price, J. V. Badding, and A. C. Peacock, "Four-wave mixing and octave-spanning supercontinuum generation in a small core hydrogenated amorphous silicon fiber pumped in the mid-infrared," *Opt. Lett.*, vol. 39, no. 19, pp. 5721–5724, Oct. 2014.
- [9] I. Hartl, X. D. Li, C. Chudoba, R. K. Ghanta, T. H. Ko, and J. G. Fujimoto, "Ultra-high-resolution optical coherence tomography using continuum generation in an air-silica microstructure optical fiber" *Opt. Lett.*, vol. 26, no. 9, pp. 608–610, May. 2001.
- [10] A. Agrawal, M. Tiwari, Y. O. Azabi, V. Janyani, B. M. A. Rahman, and K. T. V. Grattan, "Ultrabroad supercontinuum generation in a tellurite equiangular spiral photonic crystal fiber," *J. Mod. Opt.*, vol. 60, no. 12, pp. 956–962, Aug. 2013.
- [11] C. R. Phillips, C. Langrock, M. M. Fejer, J. Jiang, I. Hartl, and M. E. Fermann, "Supercontinuum generation near 2 μm in periodically poled lithium niobate waveguides," *Laser Applications to Photonic Applications (CLEO:2011)*, pp. 1-2, May. 2011.
- [12] B. Kuyken, X. Liu, R. M. Osgood, R. Baets, G. Roelkens, and W. M. J. Green, "Mid-infrared to telecom-band supercontinuum generation in highly nonlinear silicon-on-insulator wire waveguides," *Opt. Exp.*, vol. 19, no. 21, pp. 20172–20181, Oct. 2011.
- [13] I.-W. Hsieh, X. Chen, X. Liu, J. I. Dadap, N. C. Panoiu, C. Y. Chou, F. Xia, W. M. Green, Y. A. Vlasov, and R. M. Osgood Jr., "Supercontinuum generation in silicon photonic wires," *Opt. Exp.*, vol. 15, no. 23, pp. 15242–15249, Nov. 2007.
- [14] A. C. Turner, C. Manolatu, B. S. Schmidt, M. Lipson, M. A. Foster, J. E. Sharping, and A. L. Gaeta, "Tailored anomalous group-velocity dispersion in silicon channel waveguides," *Opt. Exp.*, vol. 14, no. 10, pp. 4357–4362, May. 2006.

Ranjit Das received his B.Sc. in Physics and M.Sc. in Electronic Science from University of Calcutta, India in 2007 and 2009 respectively. He started his research career as a research fellow in the Centre for Research in Nanoscience and Nanotechnology, University of Calcutta. After that he got Ph.D. in Photonics from Dept. of Applied Optics and Photonics of University of Calcutta in 2016. He was a Postdoctoral Fellow in the City University London in the tenure December 2015 to May 2016. Presently, he is Assistant Professor of Electronics at Ramakrishna Mission Vidyamandira, Belurmath, 711 202, INDIA.

Energy Harvesting Mechanism for Network/Device

Dujendu Kumar Chowdhury, Bishal Kumar Saha, Indranil Saha, Manish Agarwal, and Swarup Kumar Mitra

Abstract—Energy Harvesting which is other way defined as a technique of power or energy generation from renewable sources i.e. from external sources (thermal energy, solar power, salinity gradients, wind energy and kinetic energy etc) which being amplified, converted and finally stored in cells/battery for application of miniature devices, autonomous devices, wireless devices in industries and commercially usage. Huge demand of energy being generated from conventional energy sources for example coal, oil, hydro electric, nuclear technology which fails to meet its required demand and supply fulfillment. Harvesting or generation of a significant amount of power for low-energy wearable or Internet of Everything (IOV) devices and equipments is increasing everyday due to enormous consumability and usage. In this work we have harnessed mechanical/vibrational energy using piezoelectrical sensor. To fabricate our energy harvesting prototype we have used piezoelectric sensor (20mm Piezo Elements Sounder Sensor Trigger Drum Disc 3.6KHZ), bridge rectifier and LED. Therefore to obtain adequate output power, a charge pumps being simulated here using two -stage charge-pump and a five -stage charge-pump. The module has been optimized for accepting different incoming power levels. Layout of the module in different sections consists of sensors, rectifier, diode-capacitor stages, and a charge pump. Simulated power has been generated using TSPICE. The prototype is also verified and checked with minimum requirement of resource which proves its cost effectiveness and portability.

Index Terms— Energy Harvesting, Piezo Electric, Charge Pump, IOV (Internet of Everything)

1 INTRODUCTION

HARVESTING of energy releases up a new world of opportunities in the field of electrical engineering with applications in consumer electronics, aerospace technology, and systems that cannot be fulfilled by wires. In several applications a wired connection is simply not implantable. Energy is already in the air/space everywhere around us, and they could be harnessed for energy/power. Energy harvesting is defined as generation of minute amounts of energy from one or more of the surrounding energy sources. Windmill, geothermal and solar energy act as alternate sources of energy. The energy initiated from natural sources, termed as renewable energy. Kilo watt and Mega Watt power level are normally harvested from renewable sources of energy; it is called macro energy harvesting technology. Moreover small energy can also be produced from those regular sources that are called micro energy harvesting. Energy harvesting technology is based on mechanical vibration, mechanical strain and stress, thermal energy from furnace, heaters and resistance sources, sun light or room light, human body, biochemical or organic sources, which can generate mW or μ W level power. Need of small

power supply is increasing greatly with time with technology and its affecting to the micro and nano fabrication levels. Our work is based on harvesting energy from vibration and compressive forces using piezoelectric material. Here displacement current is generated by varying the distance of the dielectric at nano levels. The applications of this field of study are vast. One application involves harvesting energy from sources already present in the environment. Large number of application involves transmitting an RF signal from a measured and controlled source, which reflects a power transfer from one input end to the output. Traditionally these prototypes are configured through a receiving antenna that resembles a typical trans-receiver model.

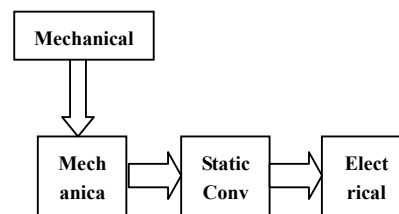


Fig. 1. Block Diagram for General Mechanical Energy Harvesting

This paper is organized as follows, in section 2 it describes the literature survey and proposed work, in section 3 it describes the results of simulated and experimental results and in

• Department of ECE, MCKV Institute of Engineering, Liluah, Howrah-711204, Email: babun.info007@gmail.com, bishalsaha623@gmail.com, rishi.saha2@gmail.com, manish1941997@gmail.com and swarup.subha@gmail.com

section 4 conclusion of the work is provided.

2 PROPOSED WORK

2.1 Literature Review

It is reported in [1], that three dissimilar devices that can be constructed into a shoe, (where excess energy is readily harvested) and used for producing electrical power "parasitically" while walking. Inertial generator [2] is established that uses thick-film piezoelectric know-hows to produce electrical power from vibrations in the environment of the device In [3] proposal, production, and testing of miniature, high-power piezoelectric firmness generators are obtainable and discussed. The work reported in [4] demonstrates a piezoelectric vibration energy generator with a power acclimatizing circuit to power a wireless sensor node. The work presented in [5] demonstrates that the power producing floors can be a main application if we use piezoelectric crystals as an energy translating material. In [6] it defines the design of energy gatherer prototype and the power preparing circuit.

2.2 Proposed Work

In our proposed work we have used vibrational energy to generate powers which exceeds all other ways of generating power. The vibrational energy generated in our work by human intervention produces better performance in track with musical instruments compared to other process[2]. Full-bridge rectifier is used as rectifier circuits to transform the AC output of a piezoelectric into a DC voltage, as shown in figure 3. The rectifying circuits consist of 4 diodes. This type of single phase rectifier uses four individual rectifying diodes connected in a closed loop "bridge" configuration to produce the desired output.

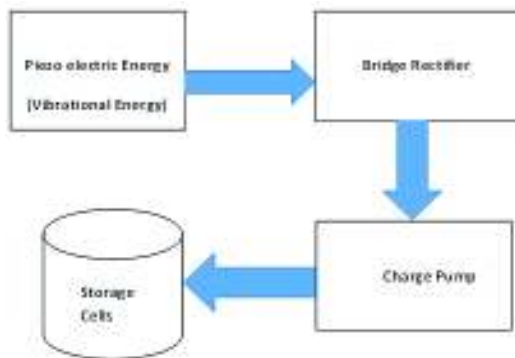


Fig. 2. Proposed Energy Harvesting Scheme

A charge pump as in fig. 2 is a kind of DC to DC converter that uses capacitors for active charge storage to bring up or down the voltage. Energy being harvested from piezo electric sensor is

rectified by full wave bridge rectifier consisting of diodes (1N4148). The output signal from the bridge rectifier is amplified using charge pump charge-pump circuits are capable of high efficiencies, sometimes as high as 90–95%, while being electrically simple circuits. The output from charge pump is transferred into a storage cell.

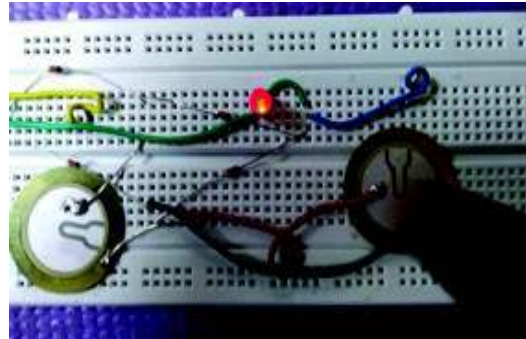


Fig. 3. Hardware implementation of Piezoelectric Generator

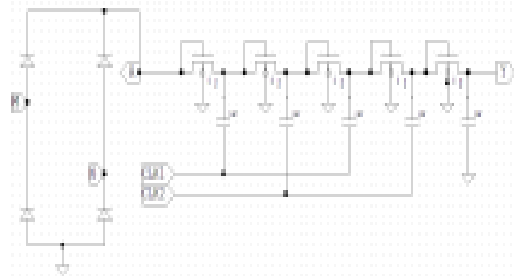


Fig. 4. Bridge Rectifier along with a Charge Pump in T-Spice

A 5-Stage charge-pump schematic is shown in Fig. 4. It functions in the following way.

- (i) During the negative half-cycles, (odd) numbered of capacitors get charged to a voltage equivalent to the input RF signal.
- (ii) Even numbered capacitors get charged in a similar way through even numbered diodes. During the positive half-cycles.

Because of the nature of diodes, where current flows from anode to cathode, they act as a one way valve, preventing the charge flowing back through the diodes.

3 RESULTS

The Simulated output waveform of the charge pump with different input combination of CLK1 and CLK2 is represented in figure 5 below.

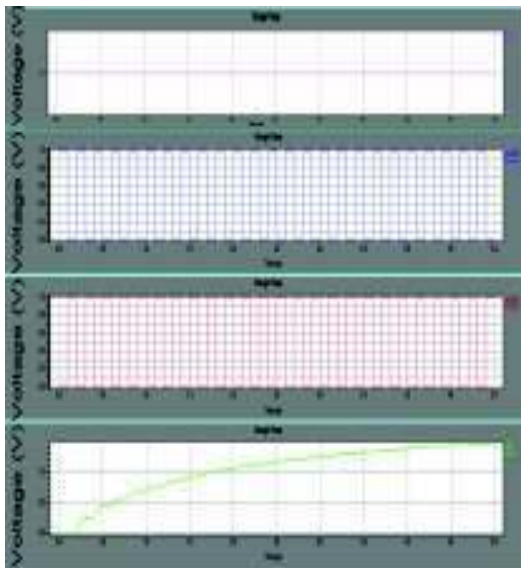


Fig. 5. Simulated Output of Charge pump with different clock pulse

Simulation Specification: The Bridge Rectifier along with the Charge Pump is implemented in the S-Edit platform using T-Spice. The layout consist of: diodes, 5 NMOS transistor stages, Capacitor(10pF), analog input (M) with substrate of NMOS transistor being connected to the ground (GND) terminal. The gate and the source terminals of all the transistors being shorted. to two clock signals(CLK1,CLK2). The input sequence of the clock signals are (CLK1={0101010101} & CLK2={1010101010}) which are inverted in nature to each other. CLK1 being applied as input to end of the Capacitors in the first and third stage (C1& C3) and CLK2 to capacitors in the second and fourth stage(let C2 & C4) respectively. The other end of the Capacitors has been connected to the drain terminals of the NMOS transistors respectively. The output has been obtained across the fifth stage of the capacitor (C5) and GND terminal. A diode rectifier bridge allow current to flow in only one direction.

Technical Conventions: Conversion of the AC voltage harvested by the piezo element into a DC voltage, are used by the capacitor as storage and the LED output in the circuit shown in fig. 3. The RadioShack diodes with a black stripe resembles the back end of the diode (convention for any 1N4148 type diode). Diodes were inserted into sockets 1A, 1B, 5C and 6A, facing the same direction with the black stripes up. Take the diode from 1A and insert the other d into socket 5A, the diode from 1B to 6B, the diode from 5C to 11C, and 6A to 11A. Connect the piezo element to the board. Inclusion of the black lead into socket 5E and the red lead into socket 6E produces a piezo electric effect. By

using LEDs, the positive side has the longer lead, and negative side with the shorter lead.

TABLE 1

Sl. No	Number of Taps	Time (t) in Seconds	Tap Frequency (TF)	Output Voltage (V)
1	10	12	0.83	0.482
2	12	9	1.33	0.658
3	15	10	1.5	1.212

Put the positive lead into socket 11E and the negative lead into 1E. LED has been hooked up to the breadboard and tapped with the piezo element. Henceforth the output being measured by intensity of the LED glow

The Output from LED as shown in fig. 3 has been measured using digital multimeter at different tap frequency and it is tabulated in table 1.

REFERENCES

- [1] J. Kymissis, C. Kendall, J. Paradiso, and N. Gershenfeld, "Parasitic power harvesting in shoes," 2nd IEEE International Conference on Wearable Computing (ISWC), pp. 132-139, 1998.
- [2] P. Glynne-Jones ; S.P. Beeby ; N.M. White, "Towards a piezoelectric vibration-powered microgenerator", IEEE Proceedings - Science, Measurement and Technology , Volume: 148 , Issue: 2 , Mar 2001.
- [3] T.G. Engel ; C. Keawboonchua ; W.C. Nunnally , "Energy conversion and high power pulse production using miniature piezoelectric compressors", IEEE Transactions on Plasma Science (Volume: 28, Issue: 5 , Oct 2000).
- [4] K. Savarimuthu, R.Sankararajan, S.Murugesan, "Design and implementation of piezoelectric energy harvesting circuit", Emerald Publishing Limited 2017.
- [5] Shreeshayana R, Raghavendra. L, Manjunath, V.Gudur, "Piezoelectric Energy Harvesting using PZT in Floor Tile Design", IJAREEIE, Vol. 6, Issue 12, December 2017, pp. 8872-8879.
- [6] Dhananjay Kumar ,Pradyumn Chaturvedi,Nupur Jejurikar, "Piezoelectric energy harvester design and power conditioning", IEEE Students' Conference on Electrical, Electronics and Computer Science, Bhopal, India, 1-2 March 2014.

Dujendu Kumar Chowdhury Final year student of B.Tech in Electronic and Communication Engineering of MCKV Institute of Engineering, Liluah, Howrah. He is the academic topper for last three consecutive years. He also has won the first prize in technical exhibition competition in Konnagar. Email ID : babun.info007@gmail.com

Bishal Kumar saha Final year student of B.Tech in Electronic and Communication Engineering of MCKV Institute of Engineering Liluah, Howrah. He also came 3rd in AISSCE 2015 class 12 (Aditya Academy Secondary

School) and came 5th in CBSE class 10 exam 2013 (Aditya Academy Secondary School). He also has achieved elite medal in NPTEL online course in introduction to internet of things and embedded system design. Email Id: bishalsaha623@gmail.com.

Indranil Saha . Final year student of B.Tech in Electronic and Communication Engineering of MCKV Institute of Engineering, Liluah, He has several innovative, novel ideas and presently working in several projects. Email Id: rishi.saha2@gmail.com.

Manish Agarwal Final year student of B.Tech in Electronic and Communication Engineering of MCKV Institute of Engineering Liluah, Howrah. He stood 1st in AISSCE 2015 class 12(Khalsa Model Senior Secondary School). and came 1st in CBSE class 10 exam 2013(school level).He also has achieved elite medal in NPTEL online course in introduction to internet of things and embedded system design. Email Id : manish1941997@gmail.com.

Swarup Kumar Mitra received his B.Tech Degree in Electronics and Tele-Communication Engineering from Kalyani University India in 2000. and has achieved his M.Tech in VLSI Design and Microelectronics Technology from Jadavpur University, India, 2007.He has more than ten years of teaching experience He is attached as Associate Professor in Department of ECE MCKV Institute of Engineering , Liluah ,Howrah India and awarded with Ph.D. (Engg.) in "Studies in Data gathering Schemes in Wireless Sensor Networks" from Jadavpur University. His present area of research is Wireless Sensor Network and its architecture etc. Email Id : swarup.subha@gmail.com

Impact of Data Normalization on Deep Neural Network for Time Series Forecasting

Samit Bhanja and Abhishek Das, *Member, IEEE*

Abstract—For the last few years it has been observed that the Deep Neural Networks (DNNs) has achieved an excellent success in image classification, speech recognition. But DNNs are suffering great deal of challenges for time series forecasting because most of the time series data are nonlinear in nature and highly dynamic in behaviour. The time series forecasting has a great impact on our socio-economic environment. Hence, to deal with these challenges its need to be redefined the DNN model and keeping this in mind, data pre-processing, network architecture and network parameters are need to be consider before feeding the data into DNN models. Data normalization is the basic data pre-processing technique form which learning is to be done. The effectiveness of time series forecasting is heavily depend on the data normalization technique. In this paper, different normalization methods are used on time series data before feeding the data into the DNN model and we try to find out the impact of each normalization technique on DNN to forecast the time series. Here the Deep Recurrent Neural Network (DRNN) is used to predict the closing index of Bombay Stock Exchange (BSE) and New York Stock Exchange (NYSE) by using BSE and NYSE time series data.

Index Terms—Neural Network, Deep Neural Network, Time Series, Data Normalization

◆

1 INTRODUCTION

FORECASTING the stock market price recently is gaining much more attention because if the successful prediction is achieved then the investors may be better guided. The profitability of the investment in stock market is highly dependable on prediction. Moreover the predicted trends also help the stock market regulator to make the corrective measure.

The Stock market is dynamic in nature and there are several complex factors that influence the market. Therefore the trends of the series are highly affected by these factors. Many researches have proposed many fundamental, technical or analytical models to predict the stock market[1]–[3] and give more or less exact prediction. There is some other linear approach such as moving average, exponential smoothening, time series regression etc. One of the most common and popular linear method is the Autoregressive integrated moving average (ARIMA)[4] model.

Artificial Neural Network (ANN) is an efficient computing system whose central theme is borrowed from the analogy of biological neural networks. The main objective of ANN[5] is to develop a system that can perform various computational tasks faster than the traditional

systems. The ANN mimic the process of human’s brain and solve the nonlinear problems, that’s why it widely used for predicting and calculating the complicated task.

Nowadays, several Artificial Neural Network (ANN) models such as Multilayer Perceptron (MLP) neural network, Back Propagation (BP)[6][7] neural networks are used to predict the stock market price.

Artificial neural networks with back propagation learning algorithm[6] are widely used in solving various classification and prediction problems. Most of the shallow networks have one hidden layer, but Deep Neural Networks (DNN)[8]–[10] have many hidden layers, and these many hidden layer allow the user to build a network model to handle highly non-linear and dynamic data and functions.

Recently deep architectures are used in various fields such as object recognition, speech recognition, natural language processing, physiological affect modelling, etc., and they provide significant performance. Unfortunately, training deep architectures is a difficult task and the classical methods are highly effective when applied to shallow architectures, but they are inefficient when they are applied on the deep architectures.

The goal of this paper is to find out the effective data normalization method to predict the Indian stock market most efficiently.

In this paper, the Deep Recurrent Neural

- Mr. Samit Bhanja is a Ph.D scholar with the Dept. of Computer Sc. & Engineering at Aliah University, Kolkata and also working as an Assistant Professor, Dept. of Computer Science, Government General Degree College, Hooghly. Email: samitbhanja@gmail.com
- Dr. Abhishek Das is Associate Professor and Head with the Dept. of Computer Science and Engineering, Aliah University, Kolkata, India. Email: adas@aliah.ac.in

Network (DRNN)[8] is used as DNN and multi attribute stock market data as Time Series data[4]. The historical stock market data are applied on DRNN to train the DRNN. The DRNN acquire the knowledge by the training process and that knowledge is applied to predict the stock market.

The organization of the paper is as follows: Section 2 provides the preliminary concept of DNN. Section 3, represents the brief description of RNNs. In Section 4, description of time series data is given. Different normalization techniques are presented in Section 5. Data set description and proposed framework is represented in the Section 6. Section 7 describes the results and discussion and finally in Section 8, the conclusion is represented.

2 PRELIMINARY CONCEPT OF DEEP NEURAL NETWORK

The term deep neural network can have several meanings, but one of the most common is to describe a neural network that has two or more layers of hidden processing neurons. These multiple layers make the DNN so efficient and effective to process the non-linear and highly dynamic data. To process these types of dynamic information, so many effective and efficient deep learning algorithms have been developed. These deep architectures are composed of many layers of non-linear processing stages, where each lower layer's output is fed into the input of next higher layer.

Originally, the concept of deep learning was developed from ANN research. Hence the MLPs or Feed-forward neural network with many layers are the good example of DNN[8]. The Back-propagation (in 1980's) is a well-known algorithm for learning weights of these types of DNNs. But, in practical it is not alone suitable for training the networks that contain more hidden layers.

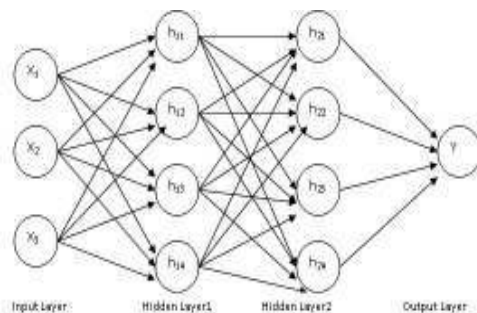


Fig. 2. A simple four layer DNN.

3 BRIEF DESCRIPTION OF RNNs

The RNNs[11] are one type deep generative architecture and they are often used to model

and generate the sequential data. They are first introduced in 1986. RNNs are very powerful for modelling sequence data (e.g., speech or text). RNNs are called recurrent because they perform the same task for every element of a sequence, with the output being dependent on the previous computations. Another way to think about RNNs is that they have a “memory” which captures information about what has been calculated so far. In theory RNNs can make use of information in arbitrarily long sequences, but in practice they are limited to looking back

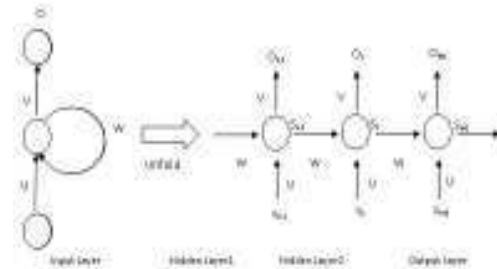


Fig.1. A recurrent neural network and the unfolding in time of the computation involved in its forward computation.

only a few steps. Here is what a typical RNN looks like:

The above diagram shows a RNN being unrolled (or unfolded) into a full network. The formulas that govern the computation happening in a RNN are as follows:

x_t is the input at time step t .

S_t is the hidden state at time step t . It's the “memory” of the network. S_t is calculated based on the previous hidden state and the input at the current step: $S_t = f(Us_t + WS_{t-1})$. The function f usually is nonlinearity such as *tanh* or *ReLU*.

O_t is the output at step t . $O_t = \text{softmax}(VS_t)$.

Unlike a traditional deep neural network, which uses different parameters at each layer, an RNN shares the same parameters (U , V , W above) across all steps. This reflects the fact that the network performs the same task at each step, just with different inputs. This greatly reduces the total number of parameters are needed to learn.

4 DESCRIPTION OF TIME SERIES DATA

A time series is a series of data collected in equal time intervals such hour, day, month, year etc. This large volume of time series data are analysed for the forecasting, such as weather forecasting, stock market prediction, Sales forecasting etc[12]–[14]. Here it is expected that value of a data X in a given time is related to the previous values. The time series is measured for

a fixed unit of time, so the series of values can be expressed as

$X = \{x(1), x(2), \dots, x(t)\}$, where $x(t)$ is the most recent value. For most of the time series problems, the goal is to forecast $x(t + 1)$ from previous values of the feature, where these values are directly related to the predicted value.

5 DIFFERENT NORMALIZATION TECHNIQUES

The effectiveness of any learning algorithm is heavily dependent on the normalization method[15]. The main objective of the data normalization method is to produce a high quality of data that can feed into any learning algorithm. The time series data can have the wide range of values, so it need to be scale to a same range of values to speed up the learning process. There are so many data normalization techniques are available. Some of them are as follows –

5.1 Min-Max Normalization

In this approach, the data scaled to a range of [0, 1] or [-1, 1]. This method convert the a input value x of the attribute X to x_{norm} the range [low, high], by using the formula-

$$x_{norm} = \frac{x - \min X}{\max X - \min X} \quad (1)$$

Where $\min X$ and $\max X$ are the minimum and maximum value of the attribute X of the input data set.

5.2 Decimal Scaling Normalization

In this technique, the decimal point of the values of the attribute is moved. This movement of the decimal point is depends on the number of digits present in the maximum value of all the values of the attribute. Hence a value x of the attribute X is converted to x_{norm} by using the formula-

$$x_{norm} = \frac{x}{10^d} \quad (2)$$

Where d is the smallest integer such that $\text{Max}(|x_{norm}|) < 1$

5.3 Z-Score Normalization

Z-Score or Standard Score converts all the values of an attribute to a common range of 0 and the standard deviation of the attribute. In this method the value x of the attribute X is converted to x_{norm} by using the formula-

$$x_{norm} = \frac{x - \mu(X)}{\delta(X)} \quad (3)$$

Where $\mu(X)$ is the mean value and $\delta(X)$ is the standard deviation of the attribute X .

5.4 Median Normalization

In this method each input value of an attribute is normalized by the median of all the values of that attribute. By using the following formula, the normalized value x_{norm} of the value x of the

attribute X can be calculated.

$$x_{norm} = \frac{x - \text{median}(X)}{\text{median}(X)} \quad (4)$$

5.5 Sigmoid Normalization

Here sigmoid function is used for the data normalization. The value x of the attribute X can be normalized by the following sigmoid function-

$$x_{norm} = \frac{1}{1 + e^{-x}} \quad (5)$$

5.6 Tanh estimators

This method is one of the most powerful and efficient normalization technique. It is introduced by Hampel. The normalized value x_{norm} of the value x of X attribute of the input data set can be calculated by the following formula-

$$x_{norm} = 0.5 \left| \tanh \left[\frac{x - \mu}{\delta} \right] + 1 \right| \quad (6)$$

Where μ and δ are mean value and standard deviation of all the values of the X attribute respectively.

6 DATA SET DESCRIPTION AND PROPOSED FRAMEWORK

As the time series data, here the stock market data are taken for the prediction. The stock market data are nonlinear and highly dynamic in nature, so it is a very challenging task to successfully predict the market hypothesis.

In this work, the Bombay Stock Exchange (BSE)[16] and New York Stock Exchange (NYSE)[17] time series data are used for the training, validation and testing purpose. The basic indices such as opening price, high price and low price are taken for the input and closing price the output.

In this work, the BSE data from 1st January 2016 to 31st December 2017 (total 493 data points) are collected. Out of these 493 data 70% of labelled data (345 data points) is used for the training, 15% of labelled data (74 data points) is used for the validation and remaining 15% unlabelled data (74 data points) are used for the testing purpose. The NYSE data from 1st January 2016 to 31st December 2017 (total 503 data points) are also collected. Out of these 503 data points 70% of labelled data (352 data points) for training purpose, 15% of labelled data (76 data points) for validation purpose and remaining 15% of data (75 data points) are used for the testing purpose.

The architecture of the proposed model depicted in the figure 3. In this model, BSE and NYSE stock market data are collected. Before applying these data into the forecasting model, the data pre-processing is done. In pre-processing phase different normalization techniques are applied to scale the data into a certain range. Then these normalized data set is used in the forecasting

model for the training, validation and testing purpose. In this work, deep recurrent neural network is used as the forecasting model.

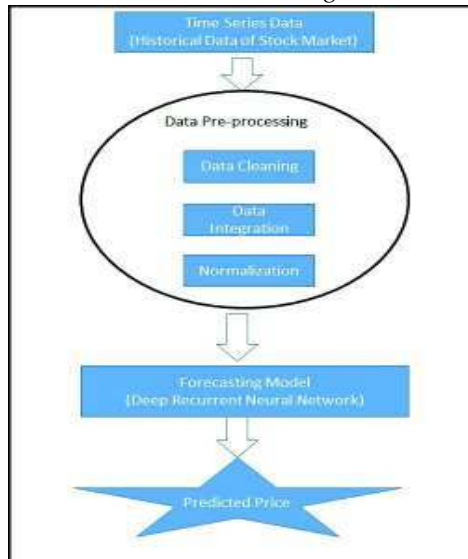


Fig.4. System Architecture

7 RESULT AND DISCUSSION

In this work, the stock indices like opening price, low price and high price are used for the input and closing price is used for the output of the network. The experiment is done using the Matlab software. The data are pre-processed by the MinMax, Decimal scaling, Z-Score, Median, Sigmoid and Tanh Estimator normalization techniques. As the forecasting model here Deep Recurrent Neural Network (DRNN) with one input layer, 20 hidden layer and output layer is used. The performance of DRNN is measured for the different normalization technique with respect to the Mean Squared Error (MSE) and Mean Absolute Error (MAE).

Fig. 4 and Fig 5 show the graph of the predicted value of the closing price versus the actual value of BSE and NYSE stock market for the different normalization techniques respectively.

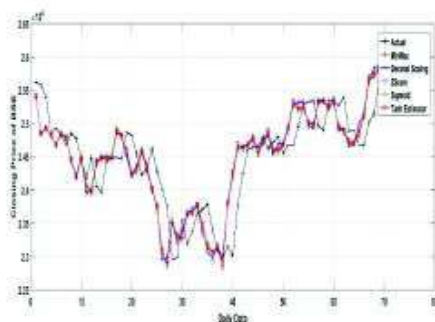


Fig. 5. Forecasting of closing price of BSE

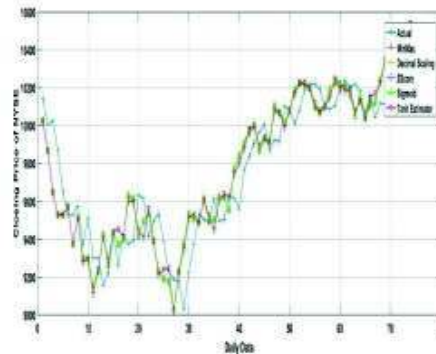


Fig. 3. Forecasting of closing price of NYSE

TABLE 1
PREDICTION ERROR OF BSE DATA FOR THE DIFFERENT NORMALIZATION METHODS

Normalization Techniques	BSE Data Set	
	MSE	MAE
MinMax	2.9079e-05	0.0040
Decimal Scaling	1.0823e-07	2.4352e-04
ZScore	3.0020e-04	0.0130
Sigmoid	2.9824e-08	1.2972e-04
Tanh Estimator	1.1537e-08	8.1233e-05

TABLE 2
PREDICTION ERROR OF NYSE DATA FOR THE DIFFERENT NORMALIZATION METHODS

Normalization Techniques	NYSE Data Set	
	MSE	MAE
MinMax	1.9097e-05	0.0033
Decimal Scaling	1.6369e-06	9.5705e-04
ZScore	2.2066e-04	0.0111
Sigmoid	7.7942e-08	2.0090e-04
Tanh Estimator	1.5486e-08	9.2140e-05

The Table 1 and Table2 shows the prediction errors such as MSE and MAE for the different normalization process for the BSE and NYSE stock market data respectively.

8 CONCLUSION

In this paper, the DRNN is applied to predict the sock index of BSE and NYSE stock market for the different normalization methods.

From the Fig.4. and Fig.5., it is observed that all the normalization techniques produced fair results.

Also, from the Table 1 and Table 2, it can be observed that all the normalization techniques produced very small amount prediction errors, but the Tanh Estimator normalization produce lasser MSE and MAE.

Thus it can be concluded that the Tanh Estimator

normalization technique is an effective normalization method for time series prediction of Deep Recurrent Neural Network.

REFERENCES

- [1] M. Farshchian and M. V. Jahan, "Stock market prediction with Hidden Markov Model," *2015 Int. Congr. Technol. Commun. Knowl.*, no. Ictck, pp. 473–477, 2015.
- [2] S. D. Bekiros, "Sign Prediction and Volatility Dynamics with Hybrid Neurofuzzy Approaches," vol. 22, no. 12, pp. 2353–2362, 2011.
- [3] F. Zhai, Q. Wen, Z. Yang, and Y. Song, "Hybrid Forecasting Model Research on Stock Data Mining," *New Trends Inf. Sci. Serv. Sci.*, pp. 630–633, 2010.
- [4] R. Adhikari and R. K. Agrawal, "An Introductory Study on Time Series Modeling and Forecasting," *arXiv1302.6613 [cs, stat]*, 2013.
- [5] V. L. Shahpazov, V. B. Velez, and L. A. Doukovska, "Design and application of Artificial Neural Networks for predicting the values of indexes on the Bulgarian Stock market," *2013 Signal Process. Symp.*, pp. 1–6, 2013.
- [6] P. J. Werbos, "Backpropagation Through Time: What It Does and How to Do It," *Proc. IEEE*, vol. 78, no. 10, pp. 1550–1560, 1990.
- [7] T. S. Lee and N. J. Chen, "Investigating the information content of non-cash-trading index futures using neural networks," *Expert Syst. Appl.*, vol. 22, no. 3, pp. 225–234, 2002.
- [8] J. Schmidhuber, "Deep Learning in neural networks: An overview," *Neural Networks*, vol. 61, pp. 85–117, 2015.
- [9] I. Chaturvedi, Y. S. Ong, and R. V. Arumugam, "Deep transfer learning for classification of time-delayed Gaussian networks," *Signal Processing*, vol. 110, pp. 250–262, 2015.
- [10] T. Villmann, M. Biehl, A. Villmann, and S. Saralajew, "Fusion of deep learning architectures, multilayer feedforward networks and learning vector quantizers for deep classification learning," in *12th International Workshop on Self-Organizing Maps and Learning Vector Quantization, Clustering and Data Visualization, WSOM 2017 - Proceedings*, 2017.
- [11] R. J. Williams and D. Zipser, "A Learning Algorithm for Continually Running Fully Recurrent Neural Networks," *Neural Comput.*, vol. 1, no. 2, pp. 270–280, 1989.
- [12] C. HSU, "FORECASTING STOCK / FUTURES PRICES BY USING NEURAL NETWORKS WITH FEATURE SELECTION," 2011.
- [13] Q. Tang and D. Gu, "Day-Ahead Electricity Prices Forecasting Using Artificial Neural Networks," *2009 Int. Conf. Artif. Intell. Comput. Intell.*, vol. 2, pp. 511–514, 2009.
- [14] M. R. Hassan and B. Nath, "Stock market forecasting using Hidden Markov Model: A new approach," in *Proceedings - 5th International Conference on Intelligent Systems Design and Applications 2005, ISDA '05, 2005*, vol. 2005, pp. 192–196.
- [15] S. C. Nayak, B. B. Misra, and H. S. Behera, "Impact of Data Normalization on Stock Index Forecasting," *Int. J. Comput. Inf. Syst. Ind. Manag. Appl.*, vol. 6, pp. 2150–7988, 2014.
- [16] "Bombay Stock Exchange." [Online]. Available: <https://in.finance.yahoo.com/quote/%5EBSESN/history?p=%5EBSESN>.
- [17] "New York Stock Exchange." [Online]. Available: <https://finance.yahoo.com/quote/%5ENYA/history?p=%5ENYA>.

Mr. Samit Bhanja is a Ph.D scholar with the Dept. of Computer Sc. & Engineering at Aliah University, Kolkata and also working as an Assistant Professor, Dept. of Computer Science, Government General Degree College, Hooghly. He has a MTech in Computer Science and Engineering.

Dr. Abhishek Das is currently working as the Head and Associate Professor in the Dept. of Computer Sc. & Engineering at Aliah University, Kolkata. His Research Area is in Medical Image Processing, Computer Vision and IoT. He has received a Post Doctoral Research position from University of West Scotland, UK by a Fellowship received from the European Commission. He has also worked as an Assistant Professor in the Dept. of Information Technology, Tripura University (A Central University), India. He has worked previously as a Reader in Computer Sc. & Engineering, Indian Institute of Space Science & Technology (IIST) and Lecturer in Information Technology, Bengal Engineering and Science University, Shibpur (now IEST Shibpur) His Ph.D is from the Dept. of Computer Sc. & Engineering, Jadavpur University, India. His M.S. in Electrical & Computer Engineering from Kansas State University, USA and B.Tech in Computer Science & Engineering from Kalyani University, India. He has worked as a Business System Analyst in Blue Cross Blue Shield New York, USA & as a Quality Analyst in Vensoft Inc. Phoenix, USA and also as a Consultant Project Manager in the Software Industry. He is also a Visiting Scientist at Indian Statistical Institute, Kolkata. He has also worked in Technical Educational Administration as Regional Officer and Asst. Director (on deputation) at AICTE (under MHRD, Govt. of India). He is a NCERT National Scholar, New Delhi and a Tilford Dow Scholar, USA. His Biography has been published in the 28th edition of National Dean's List, USA. He is a Member of IEEE and a Honorary Senior Member of IACSIT Singapore. He has several publications in International and National Journals and peer-reviewed Conferences. He is also a TPC Committee Member of IEEE International conferences in South-East Asia and Editor of the Journal of Image Processing and Pattern Recognition progress (A UGC recognised Journal) and Special Issues Journal on Image Processing & Computer Vision of IGI Global Publishers, USA (SCI and Scopus Indexed).

Reversibility of α – Asynchronous Cellular Automata: A Simulation-Based Study

Anupam Pattanayak and Subhasish Dhal

Abstract—Cellular automata (CA) is a computing model. Changes of CA cells are governed by the CA rules 0 – 255. When cells of CA are subject to change synchronously then that CA is referred as synchronous CA. But when all the cells do not participate in the process of change synchronously is called Asynchronous CA (ACA). The most complex type of ACA is α – asynchronous Cellular Automata where all the cells changes according to a probability. Reversibility is one important issue where we check if it's possible for CA with any initial state to comeback to this initial state after some time steps. We have attempted to study the reversibility of α – asynchronous cellular automata in this work which is so far not reported in the literature.

Index Terms— Cellular automata, Asynchronous cellular automata, Reversibility

1 INTRODUCTION

AMONG the many computation models proposed which are equivalent to Turing Machine is Cellular automata (CA). A simple CA is a one dimensional array (can be infinite at the both ends) of cells. Each cell is in one of a finite set of possible states at every discrete time point. Cells change state at every clock tick. If all the cells of CA can change its state at the same time then the CA is termed as synchronous CA. On the other hand If only a set of cells can change state then the CA is said to be asynchronous CA. Elementary CA (ECA, or sometimes just CA) is a 1-D CA where state of every cell is either 0 or 1 and a cell has only two neighbors - left neighbor and right neighbor [4].

ECA has 256 rules to govern the state change. If we see the truth table of the left neighbor, the cell, and right neighbor, then the output column can be one of total 256 possibilities. We refer each of these 256 possibilities of CA output as a rule. If each cell of a CA follows same rule then the CA is referred as uniform CA. When that is not the case then the CA is said non-uniform CA. In our work here, we have considered uniform ACA only. The rules are numbered according to the decimal equivalent of 8-bit binary of CA output column of the truth table. For example rule 55, which has binary equivalent 00110111, governs the change of cell of CA at time step t depending on its left and right neighbor cell to the value of cell at time step $t+1$ as per the table shown in the table 1:

- Anupam Pattanayak is Assistant Professor with the Department of Computer Science, Raja Narendra Lal Khan Women's College, Midnapore, West Bengal, India, Email: anupam.pk@gmail.com
- Subhasish Dhal is Assistant Professor with the Department of Computer Science and Engineering at Indian Institute of Information Technology Guwahati. Email: subhasis@iiitg.ac.in

TABLE 1
CA CELL UPDATE UNDER RULE 55

Leftt	Cellt	Rightt	Cellt+1
0	0	0	1
0	0	1	1
0	1	0	1
0	1	1	0
1	0	0	1
1	0	1	1
1	1	0	0
1	1	1	0

So we can express this change of a state as a local function, $f(\text{Leftt}, \text{Cellt}, \text{Rightt}) = \text{Cellt}+1$. For a given rule, if this function can be expressed using only XOR / XNOR logic functions then that CA rule is referred as linear / additive. The rules 15, 51, 60, 85, 90, 102, 105, 153, 165, 170, 195, 204, and 240 are linear. All other CA rules are nonlinear. There is one issue that points to the absence of left neighbor of leftmost cell and similarly absence of right neighbor of rightmost cell. If we consider these cells are 0 then that CA is referred as null boundary CA. If we consider that CA is circular then the CA is referred as periodic CA. In this work when we just mention CA, it means CA with periodic boundary [1].

Given a CA configuration, when all the cells undergo the transformation as per the governing rule, a new CA configuration is reached [2]. Given a CA configuration, if the CA reaches to this same configuration after two or more time steps, then the CA governing rule is said to be reversible. Reversibility of synchronous (and uniform) CA is well studied. Reversibility of ACA has attracted the few researchers to study its dynamics. But so far the existing results are available only for the fully asynchronous CA

where just one cell undergoes (possible) change. The α – asynchronous cellular automata is a more general case, where each cell undergoes the local transformation with probability α . This is more realistic to nature. There is no previous work on reversibility of α - asynchronous cellular automata in the literature as of today to the best of our knowledge.

The rest of this paper is organized as follows. Works on irreversibility of asynchronous CA and fully asynchronous CA are discussed next, in section II. Next our simulation-based observation on reversible rules for ACA is reported in section III. Finally we discuss the future scope of work and the conclusion in section IV.

2 RELATED WORK

2.1 Reversibility of Non-uniform CA

Das and Sikdar studied the reversibility of non-uniform CA with null boundary [3]. They have devised and used a tool named *reachability tree* to analyze and synthesize the reversible rules. They have listed total sixty two rules as reversible, given in the table 2.

TABLE 2
REVERSIBLE RULES FOR NON-UNIFORM NULL BOUNDARY CA

15, 23, 27, 30, 39, 43, 45, 51, 53, 54, 57, 58, 60, 75, 77, 78, 83, 85, 86, 89, 90, 92, 99, 101, 102, 105, 106, 108, 113, 114, 120, 135, 141, 142, 147, 149, 150, 153, 154, 156, 163, 165, 166, 169, 170, 172, 177, 178, 180, 195, 197, 198, 201, 202, 204, 210, 212, 216, 225, 228, 232, 240

2.2 Irreversibility of Asynchronous CA

Sarkar, Mukherjee, and Das attempted to study reversibility of ACA [5]. In order to do that they first studied separately the irreversibility of periodic ACA and irreversibility of null-boundary ACA. In the following table 3 and table 4 we list these irreversible rules respectively.

TABLE 3
IRREVERSIBLE RULES FOR PERIODIC BOUNDARY ACA

0, 2, 4, 6, 8, 10, 12, 14, 16, 20, 24, 28, 64, 66, 68, 70, 72, 74, 76, 78, 80, 84, 88, 92, 141, 143, 157, 159, 173, 175, 189, 191, 197, 199, 205, 207, 213, 215, 221, 223, 229, 231, 237, 239, 245, 247, 253, 255

TABLE 4
IRREVERSIBLE RULES FOR NULL-BOUNDARY ACA

0, 4, 13, 15, 29, 31, 45, 47, 61, 63, 69, 71, 77, 79, 85, 87, 93, 95, 101, 103, 109, 111, 117, 119, 125, 127, 141, 143, 157, 159, 160, 168, 170, 173, 175, 189, 191, 197, 199, 205, 207, 213, 215, 221, 223, 224, 229, 231, 232, 234, 237, 239, 240, 245, 247, 248, 250, 253, 255

So they were able to conclude that reversible ACA rules will not belong to this rule set. But they failed to deterministically point out the reversible rules for ACA. They remarked that “it is hard to synthesize reversible 1-d ACAs”.

2.3 Reversibility of Fully Asynchronous CA

To overcome the difficulty of synthesizing the reversibility of 1-d ACA, a special type of ACA has been considered by Sethi, Fates, and Das [6]. They have considered the ACA where just one cell is chosen for possible update at a time step. This class of ACA is referred as *fully asynchronous CA*. They have studied the reversibility of this fully asynchronous CA. They found that some rules are always irreversible. Some rules are sometimes reversible but not other times, depending on the initial state of CA. And some rules are always reversible, irrespective of initial state of CA. They have referred the class of rules which are always reversible as recurrent rules. They have found total forty six recurrent rules for fully asynchronous CA, listed in the table 5.

TABLE 5
RECURRENT RULES FOR FULLY ASYNCHRONOUS CA

33, 35, 38, 41, 43, 46, 49, 51, 52, 54, 57, 59, 60, 62, 97, 99, 102, 105, 107, 108, 113, 115, 116, 118, 121, 123, 131, 134, 139, 142, 145, 147, 148, 150, 153, 155, 156, 158, 195, 198, 201, 204, 209, 211, 212, 214

3 REVERSIBILITY OF ALPHA-SYNCHRONOUS CA

We recall again that α – asynchronous CA is the CA where each cell makes a state transition with a probability α independent of other cells.

To simulate the α – asynchronous CA, we have developed C program and compile it using gcc compiler and run it in Ubuntu system. This program implements the α – asynchronous CA. The program takes size of CA and local state update probability as inputs and produces all the rules that are reversible as output. We randomly initialize the ACA cells initially and then for each rule we update each cell with given probability and continue evolving the ACA for maximum 20,000 time steps to check if the initial state is reached. The value 20,000 is taken as a reasonable threshold to stop iterations and come to conclude that the particular rule is not reversible if the initial state is not reached. This value could have been set to a higher value, but that would make the program execution time beyond a reasonable one. We take different probabilities such as 0.1, 0.2, 0.3, 0.4, 0.5, 0.6, 0.7, 0.8, 0.9, 0.99, and 1.0 to see

the results. Note that when the probability is 1.0, the ACA becomes synchronous CA.

In the following we list out our observations for ACA of size 5, 6, 7, 8, 9, and 10.

TABLE 6
REVERSIBLE RULES FOR α – ACA WITH SIZE 5

ACA Size	α	Reversible Rules for different update probability	Remarks
5	0.1	33, 35, 38, 41, 43, 46, 49, 51, 52, 54, 57, 59, 60, 62, 97, 99, 102, 105, 107, 108, 113, 115, 116, 118, 121, 123, 131, 134, 139, 142, 145, 147, 148, 150, 153, 155, 156, 158, 195, 198, 201, 204, 209, 211, 212, 214	Total 46 rules
		33, 35, 38, 41, 43, 46, 49, 51, 52, 54, 57, 59, 60, 62, 97, 99, 102, 105, 107, 108, 113, 115, 116, 118, 121, 123, 131, 134, 139, 142, 145, 147, 148, 150, 153, 155, 156, 158, 195, 198, 201, 204, 209, 211, 212, 214	Total 46 rules
	0.2	33, 35, 38, 41, 43, 46, 49, 51, 52, 54, 57, 59, 60, 62, 97, 99, 102, 105, 107, 108, 113, 115, 116, 118, 121, 123, 131, 134, 139, 142, 145, 147, 148, 150, 153, 155, 156, 158, 195, 198, 201, 204, 209, 211, 212, 214	Total 46 rules
		33, 35, 38, 41, 43, 46, 49, 51, 52, 54, 57, 59, 60, 62, 97, 99, 102, 105, 107, 108, 113, 115, 116, 118, 121, 123, 131, 134, 139, 142, 145, 147, 148, 150, 153, 155, 156, 158, 195, 198, 201, 204, 209, 211, 212, 214	Total 46 rules
	0.5	33, 35, 38, 41, 43, 46, 49, 51, 52, 54, 57, 59, 60, 62, 97, 99, 102, 105, 107, 108, 113, 115, 116, 118, 121, 123, 131, 134, 139, 142, 145, 147, 148, 150, 153, 155, 156, 158, 195, 198, 201, 204, 209, 211, 212, 214	Total 46 rules
		33, 35, 38, 41, 43, 46, 49, 51, 52, 54, 57, 59, 60, 62, 97, 99, 102, 105, 107, 108, 113, 115, 116, 118, 121, 123, 131, 134, 139, 142, 145, 147, 148, 150, 153, 155, 156, 158, 195, 198, 201, 204, 209, 211, 212, 214	Total 46 rules
	0.8	33, 35, 38, 41, 43, 46, 49, 51, 52, 54, 57, 59, 60, 62, 97, 99, 102, 105, 107, 108, 113, 115, 116, 118, 121, 123, 131, 134, 139, 142, 145, 147, 148, 150, 153, 155, 156, 158, 195, 198, 201, 204, 209, 211, 212, 214	Total 46 rules
		33, 35, 38, 41, 43, 46, 49, 51, 52, 54, 57, 59, 60, 62, 97, 99, 102, 105, 107, 108, 113, 115, 116, 118, 121, 123, 131, 134, 139, 142, 145, 147, 148, 150, 153, 155, 156, 158, 195, 198, 201, 204, 209, 211, 212, 214	Total 46 rules
	0.9	33, 35, 38, 41, 43, 46, 49, 51, 52, 54, 57, 59, 60, 62, 97, 99, 102, 105, 107, 108, 113, 115, 116, 118, 121, 123, 131, 134, 139, 142, 145, 147, 148, 150, 153, 155, 156, 158, 195, 198, 201, 204, 209, 211, 212, 214	Total 46 rules
		33, 35, 38, 41, 43, 46, 49, 51, 52, 54, 57, 59, 60, 62, 97, 99, 102, 105, 107, 108, 113, 115, 116, 118, 121, 123, 131, 134, 139, 142, 145, 147, 148, 150, 153, 155, 156, 158, 195, 198, 201, 204, 209, 211, 212, 214	Total 46 rules
0.99	46, 51, 54, 57, 60, 62, 99, 102, 105, 108, 118, 134, 142, 145, 147, 148, 150, 153, 155, 156, 158, 195, 198, 201, 204, 212, 214	Total 27 rules	
	51, 54, 57, 60, 99, 102, 105, 108, 147, 150, 153, 156, 158, 195, 198, 201, 204	Total 16 rules	

TABLE 7
REVERSIBLE RULES FOR α – ACA WITH SIZE 6

ACA Size	α	Reversible Rules for different update probability	Remarks
6	0.1	33, 35, 38, 41, 43, 46, 49, 51, 52, 54, 57, 59, 60, 62, 97, 99, 102, 105, 107, 108, 113, 115, 116, 118, 121, 123, 131, 134, 139, 142, 145, 147, 148, 150, 153, 155, 156, 158, 195, 198,	Total 46 rules
		33, 35, 38, 41, 43, 46, 49, 51, 52, 54, 57, 59, 60, 62, 97, 99, 102, 105, 107, 108, 113, 115, 116, 118, 121, 123, 131, 134, 139, 142, 145, 147, 148, 150, 153, 155, 156, 158, 195, 198,	Total 46 rules

7	0.4	201, 204, 209, 211, 212, 214	Total 46 rules
		33, 35, 38, 41, 43, 46, 49, 51, 52, 54, 57, 59, 60, 62, 97, 99, 102, 105, 107, 108, 113, 115, 116, 118, 121, 123, 131, 134, 139, 142, 145, 147, 148, 150, 153, 155, 156, 158, 195, 198, 201, 204, 209, 211, 212, 214	
	0.6	33, 35, 38, 41, 43, 46, 49, 51, 52, 54, 57, 59, 60, 62, 97, 99, 102, 105, 107, 108, 113, 115, 116, 118, 121, 123, 131, 134, 139, 142, 145, 147, 148, 150, 153, 155, 156, 158, 195, 198, 201, 204, 209, 211, 212, 214	Total 46 rules
		33, 35, 38, 41, 43, 46, 49, 51, 52, 54, 57, 59, 60, 62, 97, 99, 102, 105, 107, 108, 113, 115, 116, 118, 121, 123, 131, 134, 139, 142, 145, 147, 148, 150, 153, 155, 156, 158, 195, 198, 201, 204, 209, 211, 212, 214	Total 46 rules
	0.8	33, 35, 38, 41, 43, 46, 49, 51, 52, 54, 57, 59, 60, 62, 97, 99, 102, 105, 107, 108, 113, 115, 116, 118, 121, 123, 131, 134, 139, 142, 145, 147, 148, 150, 153, 155, 156, 158, 195, 198, 201, 204, 209, 211, 212, 214	Total 46 rules
		33, 35, 38, 41, 43, 46, 49, 51, 52, 54, 57, 59, 60, 62, 97, 99, 102, 105, 107, 108, 113, 115, 116, 118, 121, 123, 131, 134, 139, 142, 145, 147, 148, 150, 153, 155, 156, 158, 195, 198, 201, 204, 209, 211, 212, 214	Total 46 rules
	0.9	33, 35, 38, 41, 43, 46, 49, 51, 52, 54, 57, 59, 60, 62, 97, 99, 102, 105, 107, 108, 113, 115, 116, 118, 121, 123, 131, 134, 139, 142, 145, 147, 148, 150, 153, 155, 156, 158, 195, 198, 201, 204, 209, 211, 212, 214	Total 46 rules
		38, 51, 54, 57, 60, 99, 102, 105, 108, 134, 142, 147, 148, 150, 153, 156, 158, 195, 198, 201, 204, 212, 214	Total 23 rules
	0.999	51, 54, 57, 60, 99, 102, 105, 108, 142, 147, 148, 150, 153, 156, 195, 198, 201, 204, 212, 214	Total 20 rules
		51, 54, 57, 60, 99, 102, 105, 108, 147, 150, 153, 156, 195, 198, 201, 204	Total 16 rules

TABLE 8
REVERSIBLE RULES FOR α – ACA WITH SIZE 7

ACA Size	α	Reversible Rules for different update probability	Remarks
7	0.1	33, 35, 38, 41, 43, 46, 49, 51, 52, 54, 57, 59, 60, 62, 97, 99, 102, 105, 107, 108, 113, 115, 116, 118, 121, 123, 131, 134, 139, 142, 145, 147, 148, 150, 153, 155, 156, 158, 195, 198, 201, 204, 209, 211, 212, 214	Total 46 rules
		33, 35, 38, 41, 43, 46, 49, 51, 52, 54, 57, 59, 60, 62, 97, 99, 102, 105, 107, 108, 113, 115, 116, 118, 121, 123, 131, 134, 139, 142, 145, 147, 148, 150, 153, 155, 156, 158, 195, 198, 201, 204, 209, 211, 212, 214	Total 46 rules

0.5	214	Total 46 rules	0.5	33, 35, 38, 41, 43, 46, 49, 51, 52, 54, 57, 59, 60, 62, 97, 99, 102, 105, 107, 108, 113, 115, 116, 118, 121, 123, 131, 134, 139, 142, 145, 147, 148, 150, 153, 155, 156, 158, 195, 198, 201, 204, 209, 211, 212, 214	Total 46 rules		
	35, 38, 41, 43, 46, 49, 51, 52, 54, 57, 59, 60, 62, 99, 102, 105, 107, 108, 113, 115, 116, 118, 121, 131, 134, 139, 142, 145, 147, 148, 150, 153, 155, 156, 158, 195, 198, 201, 204, 209, 211, 212, 214			Total 43 rules			
	51, 54, 57, 60, 99, 102, 105, 108, 134, 142, 147, 148, 150, 153, 156, 158, 195, 198, 201, 204, 212, 214					Total 22 rules	
	38, 51, 54, 57, 60, 99, 102, 105, 108, 134, 142, 147, 148, 150, 153, 156, 158, 195, 198, 201, 204, 212, 214						Total 23 rules
	51, 54, 57, 60, 99, 102, 105, 108, 147, 150, 153, 156, 195, 198, 201, 204						

TABLE 9
REVERSIBLE RULES FOR α – ACA WITH SIZE 8

ACA Size	α	Reversible Rules for different update probability	Remarks			
8	0.1	33, 35, 38, 41, 43, 46, 49, 51, 52, 54, 57, 59, 60, 62, 97, 99, 102, 105, 107, 108, 113, 115, 116, 118, 121, 123, 131, 134, 139, 142, 145, 147, 148, 150, 153, 155, 156, 158, 195, 198, 201, 204, 209, 211, 212, 214	Total 46 rules			
		33, 35, 38, 41, 43, 46, 49, 51, 52, 54, 57, 59, 60, 62, 97, 99, 102, 105, 107, 108, 113, 115, 116, 118, 121, 123, 131, 134, 139, 142, 145, 147, 148, 150, 153, 155, 156, 158, 195, 198, 201, 204, 209, 211, 212, 214		Total 46 rules		
		33, 35, 38, 41, 43, 46, 49, 51, 52, 54, 57, 59, 60, 62, 97, 99, 102, 105, 107, 108, 113, 115, 116, 118, 121, 123, 131, 134, 139, 142, 145, 147, 148, 150, 153, 155, 156, 158, 195, 198, 201, 204, 209, 211, 212, 214			Total 46 rules	
		33, 35, 38, 41, 43, 46, 49, 51, 52, 54, 57, 59, 60, 62, 97, 99, 102, 105, 107, 108, 113, 115, 116, 118, 121, 123, 131, 134, 139, 142, 145, 147, 148, 150, 153, 155, 156, 158, 195, 198, 201, 204, 209, 211, 212, 214				Total 46 rules
		33, 35, 38, 41, 43, 46, 49, 51, 52, 54, 57, 59, 60, 62, 97, 99, 102, 105, 107, 108, 113, 115, 116, 118, 121, 123, 131, 134, 139, 142, 145, 147, 148, 150, 153, 155, 156, 158, 195, 198, 201, 204, 209, 211, 212, 214				

0.5	33, 35, 38, 41, 43, 46, 49, 51, 52, 54, 57, 59, 60, 62, 97, 99, 102, 105, 107, 108, 113, 115, 116, 118, 121, 123, 131, 134, 139, 142, 145, 147, 148, 150, 153, 155, 156, 158, 195, 198, 201, 204, 209, 211, 212, 214	Total 46 rules			
	33, 35, 38, 41, 43, 46, 49, 51, 52, 54, 57, 59, 60, 97, 99, 102, 105, 107, 108, 113, 115, 116, 118, 131, 134, 139, 142, 145, 147, 148, 150, 153, 155, 156, 158, 195, 198, 201, 204, 209, 211, 212, 214		Total 43 rules		
	33, 35, 38, 41, 43, 46, 49, 51, 52, 54, 57, 59, 60, 97, 99, 102, 105, 107, 108, 113, 115, 116, 118, 121, 131, 134, 139, 142, 145, 147, 148, 150, 153, 155, 156, 158, 195, 198, 201, 204, 209, 211, 212, 214			Total 44 rules	
	35, 38, 41, 43, 46, 49, 51, 52, 54, 57, 59, 60, 97, 99, 102, 105, 107, 108, 113, 115, 116, 118, 121, 131, 134, 139, 142, 145, 147, 148, 150, 153, 155, 156, 158, 195, 198, 201, 204, 209, 211, 212, 214				Total 42 rules
	35, 38, 41, 43, 46, 49, 51, 52, 54, 57, 59, 99, 102, 107, 108, 113, 115, 116, 118, 115, 116, 118, 131, 134, 139, 142, 145, 153, 155, 156, 158, 195, 198, 201, 204, 211, 212, 214				

TABLE 10
REVERSIBLE RULES FOR α – ACA WITH SIZE 9

ACA Size	α	Reversible Rules for different update probability	Remarks		
9	0.1	35, 38, 43, 46, 49, 51, 52, 54, 57, 59, 60, 97, 99, 102, 105, 107, 108, 113, 115, 116, 134, 139, 142, 147, 148, 150, 153, 155, 156, 158, 195, 198, 201, 204, 209, 211, 212, 214	Total 38 rules		
		35, 38, 43, 46, 49, 51, 52, 54, 57, 59, 60, 97, 99, 102, 105, 107, 108, 113, 115, 116, 134, 139, 142, 147, 148, 150, 153, 155, 156, 158, 195, 198, 201, 204, 209, 211, 212, 214		Total 38 rules	
		35, 38, 43, 46, 49, 51, 52, 54, 57, 59, 60, 97, 99, 102, 105, 107, 108, 113, 115, 116, 134, 139, 142, 147, 148, 150, 153, 155, 156, 158, 195, 198, 201, 204, 209, 211, 212, 214			Total 38 rules
		35, 38, 43, 46, 49, 51, 52, 54, 57, 59, 60, 97, 99, 102, 105, 107, 108, 113, 115, 116, 134, 139, 142, 147, 148, 150, 153, 155, 156, 158, 195, 198, 201, 204, 209, 211, 212, 214			

		156, 158, 195, 198, 201, 204, 209, 211, 212, 214				139, 142, 147, 148, 150, 153, 156, 158, 195, 198, 201, 204, 209, 212, 214	
		35, 38, 41, 43, 46, 49, 51, 52, 54, 57, 59, 60, 97, 99, 102, 105, 107, 108, 113, 115, 116, 118, 121, 134, 139, 142, 145, 147, 148, 150, 153, 155, 156, 158, 195, 198, 201, 204, 209, 211, 212, 214	Total 42 rules	0.3		35, 43, 46, 49, 51, 54, 57, 59, 60, 97, 99, 102, 105, 108, 113, 115, 116, 118, 121, 134, 139, 142, 147, 148, 150, 153, 155, 156, 198, 201, 204, 209, 212, 214	Total 32 rules
		35, 38, 41, 43, 46, 49, 51, 52, 54, 57, 59, 60, 97, 99, 102, 105, 107, 108, 113, 115, 116, 118, 121, 134, 139, 142, 145, 147, 148, 150, 153, 155, 156, 158, 195, 198, 201, 204, 209, 211, 212, 214	Total 42 rules	0.4		35, 41, 43, 46, 49, 51, 54, 57, 59, 60, 97, 99, 102, 105, 107, 108, 113, 115, 116, 118, 121, 134, 139, 142, 145, 147, 148, 150, 153, 155, 156, 158, 195, 198, 201, 204, 209, 212, 214	Total 36 rules
		35, 41, 43, 46, 49, 51, 52, 54, 57, 59, 60, 97, 99, 102, 105, 107, 108, 113, 115, 116, 118, 121, 134, 139, 142, 145, 147, 148, 150, 153, 155, 156, 158, 195, 198, 201, 204, 209, 211, 212, 214	Total 41 rules	0.5		35, 41, 43, 46, 49, 51, 54, 57, 59, 60, 97, 99, 102, 105, 108, 113, 115, 116, 118, 121, 134, 139, 142, 147, 148, 150, 153, 156, 158, 195, 198, 201, 204, 209, 212, 214	Total 36 rules
		35, 38, 41, 43, 46, 49, 51, 54, 57, 59, 60, 97, 99, 102, 105, 107, 108, 113, 115, 116, 118, 121, 134, 139, 142, 145, 147, 148, 150, 153, 155, 156, 158, 195, 198, 201, 204, 209, 211, 212, 214	Total 41 rules	0.6		35, 43, 49, 51, 54, 57, 59, 60, 99, 102, 105, 108, 113, 115, 118, 142, 145, 147, 148, 150, 153, 156, 195, 198, 201, 204, 209, 212, 214	Total 29 rules
		35, 38, 41, 43, 46, 49, 51, 52, 54, 57, 59, 60, 97, 99, 102, 105, 107, 108, 113, 115, 116, 118, 121, 134, 139, 142, 145, 147, 148, 150, 153, 155, 156, 158, 195, 198, 201, 204, 209, 211, 212, 214	Total 41 rules	0.7		51, 54, 57, 60, 99, 102, 105, 108, 118, 134, 142, 145, 147, 148, 150, 153, 156, 195, 198, 201, 204, 209, 212, 214	Total 24 rules
		35, 38, 41, 43, 46, 49, 51, 52, 54, 57, 59, 60, 97, 99, 102, 105, 107, 108, 113, 115, 116, 118, 121, 134, 139, 142, 145, 147, 148, 150, 153, 156, 158, 195, 198, 201, 204, 209, 211, 212, 214	Total 41 rules	0.8		51, 54, 57, 60, 99, 102, 105, 108, 142, 145, 148, 150, 153, 156, 195, 198, 201, 204, 209, 212, 214	Total 21 rules
		35, 38, 43, 46, 49, 51, 54, 57, 59, 60, 97, 99, 102, 105, 108, 113, 115, 116, 118, 134, 139, 142, 145, 147, 148, 150, 153, 156, 158, 195, 198, 201, 204, 209, 211, 212, 214	Total 38 rules	0.9		51, 54, 57, 60, 99, 102, 105, 108, 147, 148, 150, 153, 156, 195, 198, 201, 204, 212, 214	Total 16 rules
		35, 51, 52, 54, 57, 59, 99, 102, 108, 118, 131, 134, 142, 145, 147, 148, 150, 153, 156, 158, 195, 198, 201, 204, 212, 214	Total 25 rules	0.99			
		51, 54, 57, 60, 99, 102, 105, 108, 147, 148, 150, 153, 156, 195, 198, 201, 204, 212, 214	Total 25 rules	0.999			
		51, 54, 57, 60, 99, 102, 105, 108, 150, 153, 156, 195, 198, 201, 204	Total 15 rules	1.0			
		51, 54, 57, 60, 99, 102, 105, 108, 147, 150, 153, 156, 195, 198, 201, 204	Total 16 rules				

TABLE 11
REVERSIBLE RULES FOR α – ACA WITH SIZE 10

ACA Size	α	Reversible Rules for different update probability	Remarks
10	0.1	35, 43, 46, 49, 51, 54, 57, 59, 60, 99, 102, 105, 108, 113, 115, 116,	Total 31 rules

4 CONCLUSION

So we observed the behavior of α – ACA for different sizes and different probabilities. We have noted down the reversible rules as per our simulation result. The result we obtain does not allow us to deterministically list the reversible rules for α – ACA like the similar works for other kind of CA. What we conclude is that it's indeed hard to synthesize the reversible rules of α – ACA. But still, we have attempted and tried to note down the results of our simulation. This we believe will pave the path for further research in this area. As a future work, we can attempt to move one step forward than fully asynchronous CA where at a time at max. Two cells can update and observe the reversibility of this kind of ACA.

ACKNOWLEDGMENT

The authors wish to acknowledge the immense help received from *Cellular Automata Research Group* of Information Technology department of IEST Shibpur for introducing this area of research and insightful discussions during 2014-15.

REFERENCES

- [1] P. Pal Chaudhury, D. Roy Chowdhury, S. Nandi, and S. Chatterjee. *Additive Cellular Automata – Theory and Applications*, volume 1. IEEE Computer Society Press, USA, 1997.
- [2] P. Sarkar, “A brief history of cellular automata,” *ACM Computing Service*, Volume 32, Issue 1., 2000.
- [3] S. Das and B. K. Sikdar, “Analysis and synthesis of nonlinear reversible cellular automata in linear time”, arXiv preprint arXiv:1311.6879, 2013.
- [4] S. Wolfram. *Cellular Automata and Complexity – Collected Papers*, Addison Wesley, 1994.
- [5] A. Sarkar, A. Mukherjee, and S. Das. “Reversibility in asynchronous cellular automata”, *Complex Systems*, 21(1):71-84, 2012.
- [6] B. Sethi, N. Fates and S. Das, “Reversibility of Elementary Cellular Automata Under Fully Asynchronous Update”, *Theory and Applications of Models of Computation*, TATM 2014, pp 39-49, 2014.

Anupam Pattanayak is an Assistant Professor in the Department of Computer Science of Raja Narendralal Khan Women's College (Autonomous), Midnapore. He has obtained B. Sc. degree in Computer Science (Honours) from Vidyasagar University in 1999. He has completed MCA degree from Swami Ramanand Teerth Marathwada University, Nanded. He has obtained M.Tech. in CSE from NIT Rourkela in 2009. He is continuing his Ph. D. in IIT Guwahati. He has worked as project-linked personnel in Applied Statistics Unit, ISI Kolkata during June 2002 – March 2004, and August 2004 – March 2005. He has also worked as part-time lecturer in Sarsuna College during September 2004 – July 2007. He has served Haldia Institute of Technology as Assistant Professor in CSE during July 2009 – December 2016. His research interests are in the areas of Information Security and Cellular Automata.

Subhasish Dhal is an Assistant Professor in the department of Computer Science and Engineering at Indian Institute of Information Technology Guwahati. He received B. Sc. degree in Computer Science (Honours) from Vidyasagar University in 2002. He has obtained his MCA degree from NIT Durgapur in 2005. He completed M. Tech. in CSE from NIT Rourkela in 2009. He has completed his PhD in IIT Kharagpur in 2016. From August 2005 till August 2007 he worked in Asutosh College, Kolkata as a lecturer and from August 2009 till December 2009, he worked in IE & IT, Durgapur as a lecturer. His research interests are in the areas of Security and privacy in IoT, Mobile Networks and Key Management and Distribution.

Detection of Fabrication, Replay and Suppression Attack in VANET- A Database Approach

Atanu Mondal and Mayurakshi Jana

Abstract—Road safety is a crucial issue in vehicular ad hoc network. The biggest challenge is safety of human life being it precious. Hence nowadays it becomes mandate the hassle free traffic which in turn can only be implemented by removing the different types of attacks in vehicular ad hoc network. The present work emphasize on identification of such three attacks such as fabrication, replay and suppression. The performance of the proposed work is also evaluated in terms of qualitatively and quantitatively which shows comparatively better performances compared to existing works.

Index Terms—Vehicular ad hoc network, vehicle identification number, certifying authority, certificate revocation list



1 INTRODUCTION

THE vehicular ad hoc network (VANET) is an emerging technology that allows vehicles on roads to communicate for driving safety. The inter vehicle communication helps to improve vehicle passenger's safety in VANET. The malicious vehicles can adversely impact this process either by replaying or by suppressing the safety messages. They may send false information to other vehicles for selfish reasons like to clear the road. Hence VANET must be protected from unauthorized message injection, message alteration which is formally known as fabrication attack, replay attack and suppression attack.

The present work is the detection of fabrication attack, replay attack and suppression attack in VANET. It also identifies the attackers and does not allocate any resource to the attackers for inter vehicle communication. The proposed VANET is a hierarchy having certifying authority (CA) at the root level, base stations (BSs) at the intermediate level and vehicles at the leaf level. Each vehicle has an electronic license plate (ELP) in which its vehicle identification number (VIN) is embedded in encrypted form (E_VIN). The ELP of a vehicle broadcasts the E_VIN after entering into the coverage area of a new BS. The BS verifies the authentication of the vehicle after receiving its E_VIN and assigns a digital signature (D_Sig) to the vehicle if it is authentic [1]. Hence in the proposed VANET each authentic vehicle has a valid D_Sig.

Each vehicle sends beacon message (B_MSG) periodically and service message (S_MSG) after the occurrence of an event. In the present work one hop communication is assumed for S_MSGs. The B_MSG is of the form of (Type, Road, Current location, E_VIN, D_Sig, Observation radius) and S_MSG is of the form of (Type, Road, Current location, E_VIN, D_Sig, Event). The Type field contains 0 for B_MSG and 1 for S_MSG. Each vehicle mentions its D_Sig in each message. So the messages are generated from authentic vehicles only which helps to protect VANET from unauthorized message injection.

Each BS receives messages during inter vehicle communication from the vehicles which are within its coverage area. It maintains three modules and two indexed databases. It triggers ALGO_B algorithm after receiving a message from a vehicle within its coverage area. The ALGO_B algorithm triggers the beacon module (BEC_M) at the BS if the received message is a B_MSG and BEC_M inserts a record in beacon database (Beacon_DAT). The ALGO_B algorithm also triggers S_MSG module (SMSG_M) at the BS if the received message is S_MSG. The SMSG_M inserts a record in SMSG database (SMSG_DAT) after verifying the integrity of the received S_MSG which helps to detect fabrication attack in VANET. The SMSG_M module generates a certificate revocation list (CRL) (CRL_SMSG_M) by inserting the E_VINs of fabrication attacker. The ALGO_B algorithm triggers the attack detection module (AD_M) after the occurrence of an event within the coverage area of a BS. This module detects the presence of replay attack and suppression attack in VANET. It identifies the attackers and generates a CRL (CRL_AD_M) by inserting the E_VINs of attackers. Finally the

- A. Mondal is with the Department of Computer Science & Electronics, Ramakrishna Mission Vidyamandira, Belur Math, Howrah. E-mail: atanumondal@vidyamandira.ac.in
- M. Jana is with the Department of Computer Science, Bijoy Krishna Girls' College, Howrah. E-mail: mjcompsec@gmail.com

ALGO_B algorithm generates a CRL by performing union operation among CRL_SMSG_M and CRL_AD_M. It sends this CRL to CA.

The CA uses ALGO_C algorithm to create a CRL (CA_CRL) from the received CRLs of the BSs. The CA_CRL contains the E_VINs of the attackers. The CA broadcasts CA_CRL for the BSs under it. Each BS stores CA_CRL and not allocates any resource to the vehicles whose E_VINs are in CA_CRL.

There is a large section of research work related to the security challenges or attacks and privacy in VANETs. The major security areas where the attacks have been reported in VANET are anonymity, key management, privacy, reputation and location [2]. Most of the research works discuss the different types of attacks on the aforementioned areas as well as their consequences. The authors not only discuss the different types of attack but also state the solutions by considering a few examples and in maximum case no simulated result or comparative study with previous works is given. It is also observed in the recent literature of security issues in VANETs, that there is almost no work related to the fabrication, replay and suppression attack[3]. In addition one point is noted that there are a few works on sybil attack [4, 5, 6] but other attacks do not get such priority for discussion. In [7] authors discussed different type of attacks like DOS, DDOS, suppression, replay etc. They stated about possible solutions of these attacks just by referring some previous work. The authors in [2] analyzed the attacks that VANETs can be subjected to. They also provide a summary of the security attacks that may be launched on VANETs and the corresponding security solutions reported in the literature to mitigate those attacks. In [8], the authors reviewed some areas like security, routing, QoS, and broadcasting techniques and they highlighted the salient results achieved to date. They also pointed out that nowadays VANET requires light-weight scalable authentication framework, which is not available, that are capable of protecting vehicles form attackers infiltrating the network using fabrication, suppression and replay attack.

2 PRESENT WORK

In this section the function of vehicle, BS and CA are elaborated for v^{th} vehicle (V_v) within the coverage area of B^{th} BS (BS_B) under CA. The number of BSs under CA and the number of vehicles under BS_B are assumed as NO_OF_BS and $NO_OF_V_B$ respectively.

2.1 Function of ALGO_B Algorithm

The function of this algorithm is elaborated for the event E_a that occurs in road R_a and location L_a

within the coverage area B^{th} BS (BS_B , $1 \leq B \leq NO_OF_BS$, NO_OF_BS is the total number of BSs under CA) under CA at t^{th} instant of time. BEC_M_B is the BEC_M module, $SMSG_M_B$ is the SMSG_M module and AD_M_B is the AD_M module at BS_B . $Beacon_DAT_B$ is the Beacon_DAT (Fig.1) and $SMSG_DAT_B$ is the SMSG_DAT (Fig.2) at BS_B . The number of roads within the coverage area of BS_B is assumed as r ($R_1 \leq R_a \leq R_r$).

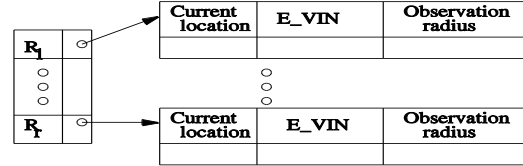


Fig.1. Beacon_DAT_B at BS_B

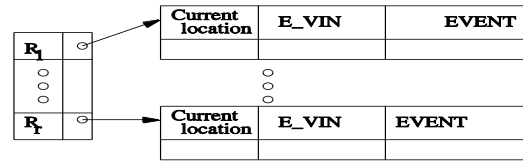


Fig.2. SMSG_DAT_B at BS_B

Let BS_B receives j^{th} message (MSG_j) from a vehicle within its coverage area and triggers ALGO_B algorithm. The ALGO_B algorithm checks the type of MSG_j . If MSG_j is of the form of $(0, R_j, L_j, E_VIN_j, D_j, OR_j)$, MSG_j is a B_MSG (B_MSG_j) and the ALGO_B algorithm triggers BEC_M_B by sending B_MSG_j .

```
/*Function of BEC_M_B for B_MSGj*/
{NB_MSG: Number of B_MSG in Beacon_DAT_B
NB_MSG ← 0
Searches Beacon_DAT_B for R_j
If found
{ Inserts a record in the data block
corresponding to R_j
NB_MSG ← NB_MSG + 1}
Else
{ Inserts a new record for R_j
NB_MSG ← NB_MSG + 1}}
```

If MSG_j is of the form of $(1, R_j, L_j, E_VIN_j, D_j, E_j)$, MSG_j is a S_MSG (S_MSG_j) which is generated for the occurrence of the event E_a and the ALGO_B algorithm triggers $SMSG_M_B$ by sending S_MSG_j . $SMSG_M_B$ switches on a timer, initializes it to τ_B and inserts all the S_MSGs that are generated for the event E_a by the vehicles in BS_B after verifying their integrity in $SMSG_DAT_B$ till the timer expires.

```
/*Function of SMSG_M_B for S_MSGj*/
{CRL_SMSG_M_B: CRL_SMSG_M at SMSG_M_B
NS_MSG: Number of S_MSG in SMSG_DAT_B
NS_MSG ← 0
If ((E_j=E_a) and (R_j=R_a) and (L_j=L_a))
{Searches SMSG_DAT_B for R_j
```

```

If found
{ Inserts a record in the data block
corresponding to Ri
NS_MSG ← NS_MSG + 1}
Else
{ Inserts a new record for Ri
NS_MSG ← NS_MSG + 1}
Else
Inserts E_VINi in CRL_SMSG_MB

```

The ALGO_B algorithm triggers AD_M_B after the occurrence of an event E_a. AD_M_B searches Beacon_DAT_B using R_a as the index. If not found there are no vehicles in the road R_a at tth instant of time and it starts to wait for the occurrence of the next event. Otherwise it searches the records corresponding to the index R_a in Beacon_DAT_B to detect the vehicles which are in road R_a and inserts the E_VIN of such vehicles in a set S_a. Let S_a = {E₁, E₂, E₄, E₆, E₉, E₁₁, E₁₂}. E₁, E₂, E₄, E₆, E₉, E₁₁, E₁₂ are the E_VINs of the vehicles V₁, V₂, V₄, V₆, V₉, V₁₁, V₁₂ respectively in road R_a at tth instant of time.

V₁ observes the event E_a if $L_a - L_1 \leq \rho_1$, where L₁ is the current location and ρ_1 is the observation radius of V₁. AD_M_B ignores V₁ if equation 1 is not satisfied. Otherwise it inserts E₁ in a set S_b and repeats the same steps of operation for the other vehicles whose E_VINs are in set S_a. Let S_b = {E₁, E₂, E₆, E₉}. So the vehicles V₁, V₂, V₆, and V₉ observe the event E_a in the road R_a.

AD_M_B also searches the data block corresponding to R_a for (E_a, L_a) in SMSG_DAT_B and creates a set S_c by inserting the E_VINs of the vehicles that generates S_MSGs for the event E_a. It counts the number of elements in S_c (Count_c) and number of elements in S_b (Count_b). If Count_b > Count_c it suspects replay attack, if Count_b > Count_c it suspects suppression attack and if Count_b = Count_c it suspects no attack.

Finally AD_M_B generates a CRL (CRL_AD_M_B) by subtracting S_b from S_c in case of replay attack and S_c from S_b in case of suppression attack.

The ALGO_B algorithm performs union operation among CRL_SMSG_M_B and CRL_AD_M_B to create CRL_B and sends CRL_B to CA. The maximum number of E_VINs in CRL_B is assumed as NEVIN_CRL_B.

2.2 Function of ALGO_C Algorithm

The ALGO_C algorithm switches on a timer and initializes it to τ_c . It receives CRLs from the BSs within its coverage area and increases a counter (NC_CRL) after receiving each CRL by 1. It stores the CRLs in a FIFO queue (Q_c) and starts to perform union operation among the received CRLs for generating CA_CRL as soon as NC_CRL becomes equal to 2 till the timer expires. The ALGO_C broadcasts CA_CRL among the BSs within its coverage area after the expiry of the timer. The maximum value of NC_CRL is

NO_OF_BS and the maximum number of E_VINs in CA_CRL is assumed as NEVIN_CA_CRL.

```

/*Function of ALGO_C algorithm*/
{ NC_CRL: Number of CRLs in Qc
NC_CRL ← 0
Switches on a timer and initializes it to  $\tau_c$ 
Receives CRL from a BS
NC_CRL ← NC_CRL + 1
Stores CRLNC_CRL in Qc
/*CRLNC_CRL: NC_CRLth CRL*/
CA_CRL ← CRLNC_CRL
LOOP:  $\tau_c = \tau_c - 1$ 
if ( $\tau_c \neq 0$ )
{Receives CRL from a BS
NC_CRL ← NC_CRL + 1
Stores CRLNC_CRL in Qc
CA_CRL ← CA_CRL U CRLNC_CRL
Go to LOOP}
else
Broadcasts CA_CRL among BSs}

```

3 SIMULATION

The performance of the proposed scheme is evaluated qualitatively and quantitatively. In this section the simulation parameters, qualitative analysis and quantitative analysis of the proposed scheme are considered for discussion.

3.1 Simulation Parameters

The size of B_MSG (Size_B_MSG) and size of S_MSG (Size_S_MSG) is the summation of the size of their attributes. The size of Type attribute is of 1 bit. Since only 0 and 1 is required to tell apart B_MSG and S_MSG. The size of Road and Current Location are assumed as 10 and 20 bits respectively to accommodate as much value as possible. The size of E_VIN (Size_E_VIN) is 17 characters [1] and the size of each character is assumed as 8 bits (extended ASCII format). Hence Size_E_VIN is 136 bits. The size of D_Sig is 160 bits [1]. The size of Observation Radius is considered as 10 bit. Since the communication range for a BS in DSRC protocol is 1 KM [9]. The size of Event for S_MSG is assumed as 6 bit to accommodate as much event as possible. Hence the Size_B_MSG and Size_S_MSG are 337 bit and 333 bit respectively. The values of τ_b , τ_c , NO_OF_BS, NEVIN_CRL_B, NEVIN_CA_CRL, NB_MSG, and NS_MSG are assumed as 30 sec, 30 sec, 3, 400, 1024, 32768, and 32768 respectively. The data transmission rate (Data_TR) is assumed as 6Mb/s [10].

3.2 Qualitative Analysis

The qualitative performance is studied on the basis of communication overhead (COMM_OH), storage overhead (STO_OH) and computation overhead (COMP_OH). The qualitative performance is evaluated by considering the total number of B_MSGs of Beacon_DAT_B as NB_MSG

after execution of BEC_{M_B}, total number of S_{MSGs} of SMSG_{DAT_B} as NS_{MSG} after execution of SMSG_{M_B} for τ_B.

Communication Overhead: The COMM_{OH} of the proposed scheme is $\sum_{B=1}^{NO_OF_BS} (COMM_OH_B) / Data_TR$ sec where COMM_{OH_B} is the COMM_{OH} of BS_B in bits. COMM_{OH_B} is due to the transmission of CRL_B to CA and reception of CA_{CRL} from CA.

Computation of COMM_{OH_B}. BS_B sends CRL_B to CA. The size of CRL_B is (NEVIN_{CRL_B} × Size_{E_VIN}) bits. Hence the communication overhead at BS_B due to the transmission of CRL_B is (NEVIN_{CRL_B} × Size_{E_VIN}) bits.

BS_B receives CA_{CRL} from CA. The size of CA_{CRL} is (NEVIN_{CA_CRL} × Size_{E_VIN}) bits. Hence the communication overhead due to the reception of CA_{CRL} is (NEVIN_{CA_CRL} × Size_{E_VIN}) bits.

Hence COMM_{OH_B} is (NEVIN_{CRL_B} + NEVIN_{CA_CRL}) × Size_{E_VIN} bits.

Storage Overhead: The storage overhead (STO_{OH}) of the proposed scheme is the sum of the storage overhead of CA (STO_{OH_CA}) and storage overhead of NO_{OF_BS} number of BSs under CA (STO_{OH_BS}).

STO_{OH_CA} is due to the storage of NO_{OF_BS} number of CRL_B in $\sum_{B=1}^{NO_OF_BS} (NEVIN_CRL_B \times Size_E_VIN) + (NEVIN_CA_CRL \times Size_E_VIN)$ bits.

STO_{OH_BS} is $\sum_{B=1}^{NO_OF_BS} STO_OH_B$ bits where STO_{OH_B} is the storage overhead of BS_B. STO_{OH_B} is due to the maintenance of Beacon_{DAT_B}, SMSG_{DAT_B} and CA_{CRL}.

Beacon_{DAT_B} has NB_{MSG} number of B_{MSGs} and hence size of Beacon_{DAT_B} is $\sum_{j=1}^{NB_MSG} Size_B_MSG_j$ bits.

SMSG_{DAT_B} has NS_{MSG} number of S_{MSGs} and hence size of SMSG_{DAT_B} is $\sum_{j=1}^{NS_MSG} Size_S_MSG_j$ bits.

CA_{CRL} has NEVIN_{CA_CRL} number of E_{VINs} and hence size of CA_{CRL} is (NEVIN_{CA_CRL} × Size_{E_VIN}) bits.

Hence STO_{OH_B} is $\sum_{j=1}^{NB_MSG} Size_B_MSG_j + \sum_{j=1}^{NS_MSG} Size_S_MSG_j + (NEVIN_CA_CRL \times Size_E_VIN)$ bits

Computation Overhead: The computation overhead (COMP_{OH}) of the proposed scheme is evaluated as the sum of the overhead of executing ALGO_B and ALGO_C algorithm.

COMP_{OH} of ALGO_B is for executing B_{MSG_B}, SMSG_{M_B}, AD_{M_B} and union operation among CRL_{MSG_{M_B}} and CRL_{AD_{M_B}}. The COMP_{OH} of B_{MSG_B} is O(NB_{MSG}). The COMP_{OH} of SMSG_{M_B} is O(NS_{MSG}). The COMP_{OH} of AD_{M_B} is O(NB_{MSG}). The COMP_{OH} of union operation among E_{VINs} of CRL_{SMSG_{M_B}} (NEVIN_{CRL_SMSG_{M_B}}) and E_{VINs} of CRL_{AD_{M_B}} (NEVIN_{CRL_AD_{M_B}})

is $O(\lceil \log(NEVIN_CRL_SMSG_M_B \times NEVIN_CRL_AD_M_B) \rceil)$.

Now the COMP_{OH} of ALGO_C is for updating NC_{CRL} and for performing union operation among the received CRLs from NO_{OF_BS} number of BSs. The computation overhead of updating NC_{CRL} for NO_{OF_BS} times is O(NO_{OF_BS}). The computation overhead of performing union operation among NO_{OF_BS} number of CRLs is $O(\lceil \log(NO_OF_BS) \rceil)$.

Hence the COMP_{OH} is O(NB_{MSG}) + O(NS_{MSG}) + $O(\lceil \log(NEVIN_CRL_SMSG_M_B \times NEVIN_CRL_AD_M_B) \rceil) + O(NO_OF_BS) + O(\lceil \log(NO_OF_BS) \rceil)$.

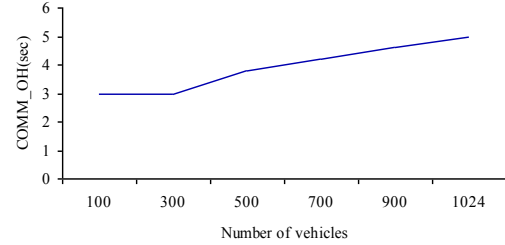


Fig. 3. COMM_OH vs. Number of vehicles

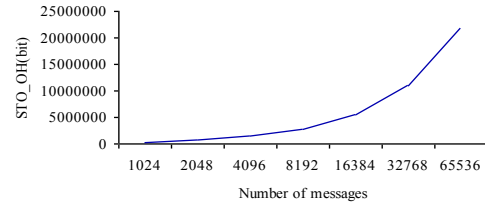


Fig. 4. STO_OH vs. Number of messages

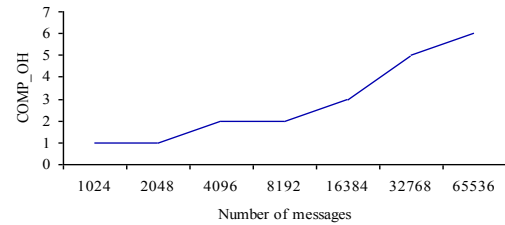


Fig. 5. COMP_OH vs. Number of messages

Fig. 3 shows the plot of COMM_{OH} vs. number of vehicles Fig.4 and Fig.5 show the plot of STO_{OH} and COMP_{OH} vs. number of messages (number of B_{MSGs} + number of S_{MSGs}) in VANET. It can be observed from Fig.1 that COMM_{OH} increases with the number of vehicles, when it becomes greater than 300. In Fig.4 it can be noticed that STO_{OH} is increased gradually with the number of messages and from Fig.5 it can be noticed that COMP_{OH} varies non-linearly with the number of messages.

3.3 Quantitative Analysis

The performance of the proposed scheme is also studied quantitatively on the basis of percentage

of message received per BS with and without the attack detection algorithm vs. simulation time. The CA_CRL distribution time (CA_CRL_DT) among BSs under CA is studied as a function of three independent variables (simulation time, rate of occurrence of event and number of vehicles) in VANET. Thus $CA_CRL_DT = F(\text{simulation time, rate of occurrence of event, number of vehicles})$.

4 CONCLUSION

To conclude it can be stated that in the present work the CA_CRL consists of E_VINs of attackers instead of their IP address like [11]. So only the E_VIN of a vehicle is sufficient to identify and detect attackers from VANET. Unlike [11] the present work performs well in high vehicle density environment. The BS receives more messages in such an environment which helps to detect attackers easily and quickly. The attack and attackers are detected by BSs in VANET. But the final CRL is generated and distributed among BSs by CA in the present work. Hence no extra task is required to assign to a vehicle for identifying attackers like [12]. Moreover the BS does not allocate any resource to the vehicles whose E_VINs are in CA_CRL which helps to utilize the available resource in VANET efficiently. Finally the proposed scheme can be extended by including a timestamp field in each S_MSG and in each record of SMSG_DAT for the detection of timing attack. The performance can be studied by considering multi hop communication of S_MSGs.

REFERENCES

- [1] A. Mondal and S. Mitra, "Identification, Authentication and Tracking Algorithm for Vehicles using VIN in Centralized VANET", International Conference on Advances in Communication, Network, and Computing, Springer LNICST, Vol. 108, pp. 279-286, 2012.
- [2] J.T. Isaac, S. Zeadally and J.S. Camara, "Security Attacks and Solutions for Vehicular Ad Hoc Networks", IET Communications, IEEE, Vol. 4, No. 7, pp. 894-903, 2010.
- [3] G. Samara, W. A. H. Al-Salihy, and R. Sures, "Security Issues and Challenges of Vehicular Ad Hoc Networks (VANET)", 4th International Conference on New Trends in Information Science and Service Science (NISS), IEEE, Jun 2010.
- [4] T. Zhou, R. R. Roy Choudhury, P. Ning and K.Chakrabarty, "P²DAP-Sybil Attacks Detection in Vehicular Ad Hoc Networks", IEEE Journal on Selected Areas in Communications, Vol. 29, pp. 582-594, 2011.
- [5] M. Rahbari and M. A. J. Jamali, "Efficient Detection of Sybil Attack Based on Cryptography in VANET", International Journal of Network Security and Its Applications (IJNSA), Vol. 3, No. 6, pp. 185-195, 2011.
- [6] S. Park, B. Aslam and D. Turgut, "Defense Against Sybil Attack in Vehicular Ad Hoc Network Based on Roadside Unit Support", Military Communication Conference, pp. 106-116, Oct 2009.
- [7] A. Rawat, S. Sharma and R. Sushil, "VANET: Security Attacks and its Possible Solutions", A. Journal of Information and Operations Management, Vol. 3, Issue 1, pp. 301-304, 2012.
- [8] S. Zeadally, R. Hunt, Y-S. Chen, A. Irwin, A. Hassan, "Vehicular AD Hoc Networks (VANETS): Status, results, and Challenges", Springer Science and Business Media, 2010.
- [9] P. Papadimitratos, G. Mezzour and J.P. Hubaux, "Certificate Revocation List Distribution in Vehicular Communication Systems", Proceedings of the Fifth ACM International Workshop on Vehicular Internetworking, pp.86-87, 2008.
- [10] O.F.G. Duque, A.M. Hadjiantonis, G. Pavlou and M. Howarth, "Adaptable Misbehavior Detection and Isolation in Wireless Ad Hoc Networks Using Policies", IFIP/IEEE International Symposium on Integrated Network Management, pp. 242-250, 2009.
- [11] K. Persad, C. M. Walton and S. Hussain, "Electronic Vehicle Identification: Industry Standards, Performance. Project 0-5217, Texas Department of Transportation, Aug 2006.
- [12] Towards Effective Vehicle Identification, The NMVTRC's Strategic Framework for Improving the Identification of Vehicles and Components (2004).

Atanu Mondal received M.Tech (CSE) degree from Calcutta University (India) in 2008 and Ph.D (Engineering) degree from Indian Institute of Engineering Science and Technology, Shibpur (India) in 2018. Dr. Mondal has published 16 technical papers in Journal and International conference proceedings. His current research interests are bioinformatics and data security. He is currently with the Computer Science and Electronics department of Ramakrishna Mission Vidyamandira, Belur Math as Assistant Professor.

Mayurakshi Jana received M.Sc degree in computer science from West Bengal State University (India) in 2016 and B.Sc degree in computer science from University Of Calcutta in 2014. She is currently with the Department of Computer science, Bijoy Krishna Girls' College, Howrah as College contractual teacher.

000101



010010111